THE ASTROPHYSICAL JOURNAL, 311:708–730, 1986 December 15

THE ASYMPTOTIC GIANT BRANCH EVOLUTION OF 1.0–3.0 $M_\odot$ STARS AS A FUNCTION OF MASS AND COMPOSITION

JOHN C. LATTANZIO
Canadian Institute for Theoretical Astrophysics, McLennan Physical Laboratories, University of Toronto
Received 1985 November 6; accepted 1986 April 14

ABSTRACT

Evolutionary calculations are presented for 1.0–3.0 $M_\odot$ stellar models covering the abundances $Z = 0.001$, 0.01, and 0.02 with $Y = 0.20$ and 0.30. Calculations are begun on either the zero-age main sequence or the zero-age horizontal branch, as appropriate, and include semiconvection in a simple but effective manner. We verify the existence of convective pulses found by Castellani *et al.* for larger masses. The evolution is continued through to the thermally pulsing Asymptotic Giant Branch stage. The core masses at the first pulse are found to be larger than previously estimated for $M \lesssim 2\ M_\odot$ and smaller than estimated for $2 \lesssim M/M_\odot \lesssim 3$. These effects may have implications for Iben's "Carbon star mystery." Indeed, taking into account Wood's results, we predict that many stars in this mass range, expecially those of lower metallicity, should begin dredging carbon to their surfaces from the first pulse. Some models have had their evolution continued until the thermal pulses reach full amplitude, enabling the derivation of a core mass–luminosity relation for this mass and abundance range. None of these models are found to experience the third dredge-up, but this is entirely due to using $\alpha = 1.0$. Comparison with some individual C stars, especially the potentially troublesome star TW Hor, shows that the models presented agree quite well with the observations, provided $\alpha \approx 1.5$.

Subject headings: clusters: globular — convection — stars: evolution — stars: interiors

I. INTRODUCTION

One of the last stages of single-star evolution to give up its secrets is that of the asymptotic giant branch (AGB) phase (for a review see Iben and Renzini 1983). Calculations of models of low-mass stars ($M \lesssim 1.0\ M_\odot$) have applications to the frequency of C stars, white dwarfs, planetary nebulae and their central stars, etc. Similarly, the study of more massive stars ($M \gtrsim 3.0\ M_\odot$) has been explored by many authors (again, see the above mentioned review). In this mass range, a systematic study of AGB evolution as a function of mass and composition has been given by Becker and Iben (1979, 1980). It is clear that we now have extensive calculations of evolutionary models from the zero-age main sequence (ZAMS) to the AGB for $M \lesssim 1.0\ M_\odot$ and for $M \gtrsim 3.0\ M_\odot$. Yet, with the exception of a few isolated cases (Paczyński 1971; Gingold 1975; Wood 1981; Wood and Zarro 1981), there are no studies in the range 1–3 $M_\odot$, certainly no systematic studies as a function of mass and composition, and only one case where the evolution has been followed from the ZAMS (or zero-age horizontal branch [ZAHB], as appropriate) through to the thermally pulsing (TP) AGB stage (Gingold 1975).

The interest in the mass range 1–3 $M_\odot$ is motivated by more than a desire for completeness. In recent years a substantial body of observational data has been built up for late M and C stars in the Magellanic Clouds (Blanco, Blanco, and McCarthy 1978; Blanco, McCarthy, and Blanco 1980; Mould and Aaronson 1979; Richer 1981; Cohen *et al.* 1981; Miller and Scalo 1982; Bessell, Wood, and Lloyd Evans 1983). The most common giant-branch stars in the Magellanic Clouds have masses ~1–2 $M_\odot$, and thus calculations in this range are necessary to provide correct input (initial hydrogen-exhausted core mass, dredge-up law, etc.) for synthetic AGB populations (Wood and Cahn 1977; Iben and Truran 1978; Iben 1981; Renzini and Voli 1981). It is now well known that these synthetic distributions fail to form C stars of low luminosity and predict too many at higher luminosities (as first suggested by Gingold 1975).

In the hope that detailed models for various masses and abundances may help determine the low-luminosity limit of the C-star distributions, this paper considers the evolution of model stars with masses in the range 1–3 $M_\odot$ and various compositions. With improved observations reaching down to the clump in observed color-magnitude diagrams for Magellanic Cloud clusters, these calculations may also serve as calibrations of clump giant models.

II. INPUT PHYSICS

The opacity tables used were constructed with the Los Alamos *Astrophysical Opacity Library* (Huebner *et al.* 1977), supplemented with the Cox and Stewart (1970*a*, *b*) values for $T < 10^4$ K, as discussed below. I also briefly discuss some calculations using opacity tables for low temperatures which were kindly provided by D. Alexander (private communication).

Evolutionary calculations were performed with the Mount Stromlo stellar structure code. The nuclear reaction chain $^{14}N(\alpha, \gamma)^{18}F(\beta^+\ \nu)^{18}O(\alpha, \gamma)^{22}Ne(\alpha, n)^{25}Mg$ was ignored in all models to be presented. Test calculations showed that including this network did not significantly alter the results. If one is interested in the production of *s*-process elements during helium shell flashes, of course, then neutrons produced via the ^{14}N-burning chain are of vital importance (e.g., Iben 1975*a*, *b*, 1976; Iben and Truran 1978).

Neutrino energy losses due to four processes are included. For plasmon decay, pair annihilation, and photoneutrino production, the rates are taken from Beaudet, Petrosian, and Salpeter (1967). The bremsstrahlung process rate is taken from Festa and Ruderman (1969). In recent years there has been growing evidence for the existence of neutral currents (Hasert *et al.* 1973; Barish *et al.* 1974; Lubkin 1978; Itzykson and Zuber 1980, and others). The Weinberg-Salam theory of the weak and electromagnetic interactions (Weinberg 1967, 1972; Salam 1968) has been included via corrections to the above rates. Ramadurai (1976) provides these corrections for the pair annihilation, photoneutrino, and plasma processes, while Dicus *et al.* (1976) provide a similar correction for the bremsstrahlung process. These corrections are defined in terms of the experimentally determined Weinberg angle θ_W. In the calculations to be presented below, we have used $\sin^2 \theta_W = 0.25$ (Lubkin 1978; Itzykson and Zuber 1980). The resulting correction factors are 1.000, 0.583, 1.000, and 0.750 for the plasma, photoneutrino, pair annihilation, and bremsstrahlung processes respectively. The inclusion of these correction factors should not significantly alter any previous results, because the dominant processes found in the interiors of AGB stars are the plasma and bremsstrahlung processes (Becker and Iben 1979; see also Festa and Ruderman 1969).

Semiconvection plays an important role in the structure of stellar models during the core helium burning phases of evolution. We have included semiconvection (and approximated convective overshooting) in the following simple but effective manner. Suppose mesh point j is the outer (inner) edge of a formally convective zone. By evaluating the radiative to adiabatic ratio $\nabla_{\rm rad}/\nabla_{\rm ad}$ at mesh point $j-1$ $(j+1)$, we can extrapolate to find $(\nabla_{\rm rad}/\nabla_{\rm ad})_{\rm extrap}$ at $j+1$ $(j-1)$. If this value is greater than unity, then we incorporate the $j+1$ $(j-1)$ mass shell into the convective zone, even though the shell may have $\nabla_{\rm rad} < \nabla_{\rm ad}$ when calculated formally. This procedure is executed, at each convective boundary, each time the abundances are mixed over a convective region. This is usually after each iteration, thus allowing for rapid growth of a convective zone through overshooting, if such is required physically. The realistic treatment of an overshooting zone is also dependent on the mesh spacing in this zone, as the smallest increment that can be added to the convective zone is one mass shell. Note, however, that the determination of convective overshooting through nonlocal effects is beyond the scope of this paper and remains an uncertainty in the models (see, however, Chiosi 1986).

Most evolutionary calculations which include the effects of semiconvection use the scheme proposed by Robertson and Faulkner (1972) or some variant thereof. In this method the abundances in the semiconvective zone are adjusted until convective neutrality is achieved via $\nabla_{\rm rad} = \nabla_{\rm ad}$. This leads to smooth abundance profiles, which will adequately reflect the average composition gradient in the zone. The actual situation will be many zones with $\nabla_{\rm rad}$ very near to $\nabla_{\rm ad}$ in value, but some convective and some radiative. Gabriel (1970) estimates the size of these zones to be $\sim 10^{-4}\ M/M_\odot$, and Sweigart and Renzini (1979) use small, discrete mixing events to explain the rapid period changes observed in RR Lyrae stars.

During the core helium burning stages of the evolution described below, we have modeled semiconvection by allowing for overshoot, as described above, and restricting the size of mass shells in the potential semiconvective zone to be of width $\Delta m/M = 0.003$. This value was chosen after a series of tests comparing the resultant abundance profiles and evolution with the results of Faulkner and Cannon (1973), who used the Robertson and Faulkner (1972) method. The agreement was excellent (see Lattanzio 1984*a* for details) and showed only a weak dependence on $\Delta m/M$. A complication arose in the calculations when the central helium abundance Y_c dropped below ~ 0.20. This is believed to be due to a physical, rather than numerical, process and is discussed below.

III. INITIAL MODELS

a) Construction

Three metallicities have been chosen, $Z = 0.02$, 0.01, and 0.001, and for each of these we take $Y = 0.20$ and 0.30. In all cases C:N:O = 3:1:9 and $Z_{\rm CNO} = 0.6Z$. The ratio of mixing length to pressure scale height $\alpha = l/H_p = 1.0$ is chosen for consistency with Becker and Iben (1979, 1980).

The evolutionary calculations may be divided into three distinct cases: M, H, and F. Case M refers to models whose evolution is begun on the ZAMS, those which do not suffer a core helium flash. This is usually taken to mean masses $\gtrsim 2.25$ $M_\odot$, but for $(Y, Z) = (0.20, 0.02)$ a core flash was found for the 2.5 $M_\odot$ model. An evolutionary sequence for a 2.6 $M_\odot$ model with the same abundances ignited helium gently. Thus a core flash is found for $M \leq 2.5\ M_\odot$ for $(Y, Z) = (0.20, 0.02)$. Obviously, the maximum mass star which experiences a core flash will depend on composition. Also, since some case M models will experience blue loops during the core helium burning phase, care was taken to obtain accurately the hydrogen profile left by the receding convective core. Typically the mesh spacing was reduced by factors of ~ 30 near the convective core edge, and convergence was tightened to one part in 10^4.

Case H evolution refers to sequences which do not suffer a core flash, and hence their evolution is begun on the ZAHB. In this case the initial core masses at a given (M, Y, Z) are interpolated within the results of Sweigart and Gross (1978). The changes in the surface abundances due to the first dredge-up episode are included. For ^{12}C, ^{14}N, and ^{18}O they were found by interpolation in the results of Lattanzio (1984*b*), neglecting the minor variations due to the different initial abundances and mixing length used in those models. The variation in the surface H and ^{4}He was found by interpolation in the Sweigart and Gross models.

For $Z = 0.001$ it was not possible to interpolate within the results of Sweigart and Gross (1978) to obtain ZAHB core masses as they only considered $M < M_\odot$ for this metallicity. In these cases the required models were evolved from the ZAMS to the core flash, and then the abundances and core masses so obtained were used to begin the evolution from the ZAHB. These models form case F. Note that the $(M, Y, Z) = (2.5, 0.20, 0.02)$ model is also a case F model, because evolution was begun on the ZAMS since a core flash was not anticipated.

Details of the initial models are given in Table 1. Note that for all models we have included the effects of the first dredge-up on the envelope abundances, either by evaluating it explicitly (cases M and F) or by estimating its effect (case H).

It was assumed that, during the helium core flash, exactly 3% by mass of helium was fused into carbon, in accord with previous estimates (Härm and Schwarzschild 1966; Iben and Rood 1970; Demarque and Mengel 1971), although Despain (1981) finds $\sim 5\%$ of helium is burnt during the core flash for a 0.6 $M_\odot$ Population II model. We should also note the hydrodynamic calculations of Cole and Deupree (1981; see also Cole and Deupree 1980; Deupree and Cole 1981, 1983; Deupree 1984*a*, *b*) who find $\sim 60\%$ of the helium core is processed into "some unspecified collection of metals." Details of the evolution through the core helium flash depend crucially on the assumptions made concerning convective heat transport, etc., and a thorough understanding of this complicated stage is still

TABLE 1

Initial Values for the Evolutionary Sequences

Y[a]	$M/M_\odot$	Start[b]	$M_c/M_\odot$[c]	ΔY_s[d]	$^{12}C_s$[e]	$^{14}N_s$[e]	$^{16}O_s$[e]
			$Z = 0.02$				
0.20..........	5.0	ZAMS	0.751	0.009	1.75 (−3)	2.40 (−3)	7.98 (−3)
0.20..........	4.0	ZAMS	0.523	0.013	1.73 (−3)	2.46 (−3)	7.94 (−3)
0.20..........	3.0	ZAMS	0.391	0.016	1.73 (−3)	2.41 (−3)	8.00 (−3)
0.20..........	2.5	Flash	0.411	0.014	1.76 (−3)	2.22 (−3)	8.17 (−3)
0.20..........	2.0	ZAHB	0.465	0.014	1.82 (−3)	2.07 (−3)	8.28 (−3)
0.20..........	1.5	ZAHB	0.479	0.020	2.02 (−3)	1.82 (−3)	8.31 (−3)
0.20..........	1.0	ZAHB	0.485	0.025	2.50 (−3)	1.24 (−3)	8.31 (−3)
0.30..........	2.5	ZAMS	0.343	0.008	1.77 (−3)	2.22 (−3)	8.16 (−3)
0.30..........	1.5	ZAHB	0.459	0.011	2.02 (−3)	1.82 (−3)	8.31 (−3)
			$Z = 0.01$				
0.20..........	2.5	ZAMS	0.320	0.015	8.44 (−3)	1.19 (−3)	4.04 (−3)
0.20..........	1.5	ZAHB	0.482	0.023	1.01 (−3)	9.08 (−4)	4.15 (−3)
0.30..........	2.5	ZAMS	0.375	0.008	8.55 (−4)	1.16 (−3)	4.06 (−3)
0.30..........	1.5	ZAHB	0.461	0.014	1.01 (−3)	9.08 (−4)	4.15 (−3)
			$Z = 0.001$				
0.20..........	3.0	ZAMS	0.441	0.002	9.63 (−5)	9.54 (−5)	4.15 (−4)
0.20..........	2.5	ZAMS	0.352	0.009	8.15 (−5)	1.14 (−4)	4.14 (−4)
0.20..........	2.0	Flash	0.452	0.021	8.21 (−5)	1.15 (−4)	4.12 (−4)
0.20..........	1.5	Flash	0.481	0.025	9.69 (−5)	9.48 (−5)	4.15 (−4)
0.20..........	1.0	Flash	0.492	0.019	1.24 (−4)	6.29 (−5)	4.15 (−4)
0.30..........	2.5	ZAMS	0.393	0.001	1.03 (−4)	8.78 (−4)	4.15 (−4)
0.30..........	1.5	Flash	0.449	0.016	9.10 (−5)	1.02 (−4)	4.15 (−4)

[a] Helium abundance on the ZAMS.
[b] Where the evolution was begun: ZAMS for case M, Flash for case F, ZAHB for case H.
[c] The core mass on the ZAHB, or when $L_{He} > 1\ L_\odot$ for models which ignite helium gently.
[d] The increase in surface helium abundance due to the first dredge-up episode.
[e] Surface abundances after the first dredge-up episode; parentheses enclose powers of factor 10.

lacking. Indeed, the Cole and Deupree calculations are not without criticism (e.g., Iben and Renzini 1983), and it seems appropriate to use the more conservative estimates of quasi-static models until the situation is clearer.

Having determined the envelope and core abundances as well as the core mass (for evolutionary cases H and F), we construct models with an abundance discontinuity at $M = M_H$, the edge of the hydrogen-exhausted core, as outlined by Castellani and Tornambe (1977; see also Caputo, Castellani, and Tornambe 1978, hereafter CT and CCT respectively). The abundance discontinuity assumed at M_H is a limiting case of the extremely thin shells found at the time of the core helium flash. It is well known that by the time the star reaches the ZAHB the shell is much wider ($\sim 10^{-2}\ M_\odot$, as opposed to $\sim 10^{-4}\ M_\odot$ on the giant branch). By allowing the abundances in the shell to "burn in" to their appropriate distribution, we make no assumption about the elemental distribution throughout the shell.

b) Early Evolution

We now briefly discuss the initial evolution from a state with abundance discontinuities at M_H to one with a smooth abundance profile. Such evolution has been discussed by CT and CCT for models with $M < M_\odot$. They found their models rapidly traversed a path to the blue, reaching a maximum T_e significantly underluminous relative to the ZAHB model, before reversing the evolutionary path. This first stage of evolution has a time scale of $\sim 10^6$ yr. The evolution then slows and reaches a time scale typical of horizontal-branch models, after decreasing Y_c by ~ 0.01 and decreasing the hydrogen abundance at the base of the hydrogen burning shell by ~ 0.05. The behavior of the more massive models considered here is similar. By this stage the abundance discontinuity has been smoothed to that expected in a shell, and ^{12}C and ^{14}N have reached equilibrium abundances throughout the shell.

IV. CORE HELIUM BURNING STAGE

a) Overlap with Previous Calculations

There is a substantial amount of literature on the core helium burning phases of stars with $M > 3\ M_\odot$ (e.g., Paczynski 1970, 1974; Becker, Iben, and Tuggle 1977, hereafter BIT; Alcock and Paczyński 1978; Becker 1981). A model with $(M, Y, Z) = (5.0, 0.20, 0.02)$ was considered by BIT. The evolution of this model was continued through the early (E) AGB phase and to the first thermal pulse by Becker and Iben (1979, 1980). Thus it was decided to also follow the evolution of an identical model to allow a comparison between evolutionary codes and to ensure compatibility with previous calculations.

The resulting evolution showed two differences when compared to the corresponding BIT model. First, the position of the ZAMS was shifted by ~ -0.06 in log $(L/L_\odot)$ and -0.02 in log T_e. This is entirely due to the different opacity tables used, as was verified by reconstructing the model with the Cox and Stewart opacity tables used by BIT. A related disparity was in the duration of core hydrogen burning, which was $\sim$30% longer in the current model. This is due to a larger convective core in my model (by $\sim$0.1 $M_\odot$), again due to the increased opacity values found in the Huebner *et al.* (1977) tables. Note also that BIT ignored semiconvection when constructing their models, whereas a not insignificant semiconvective zone was found to be present. This is consistent with the models of Robertson (1971) and Alcock and Paczyński (1978) for similar masses and abundances.

The second important difference is the extent of the blue loops during core helium burning. The new model shows a much smaller loop than found by BIT, reaching to log T_e = 3.790 at the bluest point, compared to 3.875 for the BIT model. This can be understood by following the analysis of Lauterborn, Refsdal, and Weigart (1971). We find that $\tau_{\rm core}/\tau_{\rm profile} = 2.9$ for the new model, but is 3.9 for the BIT model. Thus the new models, constructed with the higher opacity, shows a smaller loop due to the more rapid core evolution, since both sequences show essentially the same $\tau_{\rm profile}$. We note here that these changes to the extent of the blue loops may produce important changes in the period distribution of Cepheids. It is suggested that extensive pulsation and evolution calculations with the new opacity may be worthwhile.

b) Semiconvection and Helium Spikes

Semiconvection has been included in the manner previously described. An extensive comparison with previous calculations has shown that this simple method yields results which are almost indistinguishable from the more complex methods (e.g., Robertson and Faulkner 1972; see Lattanzio 1984*a* for details). A convergence problem obtained near the end of the core helium burning stage has already been briefly mentioned. It was usually these models which showed an increase in the convective core size, resulting in a rapid rise in the central helium abundance Y_c. This phenomenon has been noted by many authors (e.g., Demarque and Mengel 1972; Sweigart and Demarque 1972, 1973; Sweigart and Gross 1976; Gingold 1976; Taam, Kraft, and Suntzeff 1976; Sweigart and Renzini 1979), most recently by Castellani *et al.* (1985*a*), and corresponds to the core breathing phenomenon of Castellani, Giannone, and Renzini (1971*a*, *b*). The extra helium mixed into the core from the semiconvective zone results in a spike in the time variation of Y_c, a rapid loop in the H-R diagram, and some minor, short-lived variations in the stellar structure. Sweigart and Demarque (1973) showed that this was a physical instability caused by the triple-α reaction. A small increase δY_c in Y_c can cause a large increase in the energy generation rate, if Y_c is sufficiently small. This, in turn, causes a rapid growth in the extent of the convective core. Sweigart and Demarque found unstable cores for $Y_c \lesssim 0.12$ for low-mass ($M \lesssim M_\odot$) models. They found Y_c then rose to $\sim$0.20 over $\sim 10^6$ yr, whereas Gingold (1976) found a Y_c rise from 0.02 to 0.16 in one of his models, almost independent of the time step used. Taam, Kraft, and Suntzeff (1976) found Y_c rising to $\sim$0.17 from $\sim$0.05.

Various numerical tests were performed to determine the effect of numerical parameters on the number and size of the helium spikes. Restrictions were placed, alternatively, on the time step, the mass zone spacing, and the convergence criteria. In all cases the resulting spikes were of approximately the same size and occurred at essentially the same time. We conclude that the details of the numerical scheme are not crucial to the details of this phenomenon (details may be found in Lattanzio 1984*a*).

Castellani *et al.* (1985*b*) have performed a detailed analysis of the phenomenon of the helium spikes. Their results showed that there were usually three major helium spikes, which was verified in the results for the models presented below. The increase in the central helium abundance leads to rapid blueward loops in the H-R diagram which are short-lived features and will be suppressed from the H-R diagrams to be presented. Their main effect is to increase the core helium burning lifetime, and thus the extent of the helium-exhausted core, when central helium is finally depleted. For larger masses this can significantly decrease the maximum stellar mass which develops a degenerate carbon-oxygen core, as discussed by Castellani *et al.* (1985*a*), and required by observations (see Renzini *et al.* 1985). The similarity between my models and those of Castellani *et al.*, despite the very different prescription for treating semiconvection, again provides further confidence in the predicted behavior of real stars during the core helium exhaustion phase.

c) Overview of the Evolution

The evolution during core helium burning is governed by competition between two processes. First there is helium burning in the core, producing ^{12}C and ^{16}O, and second there is the advancement of the hydrogen burning shell, which increases the mass of the hydrogen-exhausted core, $M_{\rm H}$. Because the evolution during this phase is qualitatively well understood, we present only a brief discussion, plus the quantitative results.

Initially the hydrogen burning shell provides most of the luminosity escaping the star. The ratio $L_{\rm H}/L_{\rm He}$ decreases with time, due to two complementary effects. The energy release from the helium burning core increases as Y_c decreases. Simultaneously, the hydrogen burning shell moves outward (in both mass and radius) to lower temperatures and densities, resulting in a decrease in $L_{\rm H}$.

The core initially consists of a small formally convective region. As the evolution proceeds, the extent of this core increases until it reaches its maximum. At this stage $Y_c \approx 0.7$, and further increase in the convective zone by overshooting leads to a semiconvective region. The maximum mass of this semiconvective zone is typically half the mass contained in the formally convective core. The ^{12}C abundance in the core passes through a maximum when the ^{12}C(α, γ)^{16}O reaction grows in importance, increasing the ^{16}O content at the cost of ^{12}C. When Y_c decreases to sufficiently small values ($\lesssim$0.20), the instability previously mentioned leads to $\sim$3 helium spikes, just prior to central helium exhaustion. During the time of core helium burning, the total luminosity and effective temperature remain essentially constant for $M \lesssim 2.3$ $M_\odot$. For larger masses we see the characteristic blue loops in the H-R diagram (for an analysis of this phenomenon see Lauterborn, Refsdal, and Weigert 1971).

Table 2 gives some details of each of the evolutionary sequences. Figure 1 shows the evolutionary tracks for the $(Y, Z) = (0.20, 0.02)$ models. Tracks are not presented for all models, but Tables 3 and 4 list interesting evolutionary points and the times when they occur for all models. Note that the model with $(M, Y, Z) = (2.0, 0.20, 0.001)$ (case F, not shown) is unusual in that it is the only model which experienced both a core helium flush and a blue loop during its subsequent evolution. The small loop forms a smooth sequence between the results for the 3.0, 2.5, and 1.5 $M_\odot$ models of the same abundances.

We observe that, for constant Y and Z, helium burning

TABLE 2

EVOLUTIONARY PARAMETERS FOR THE MODEL SEQUENCES

Y	M $(M_\odot)$	$M_{cc}^{max\ a}$ $(M_\odot)$	$M_{scv}^{max\ b}$ $(M_\odot)$	t_{CHeB}[c] $(\times 10^6$ yr)	t_{CHeE}[d] $(\times 10^6$ yr)	$^{12}C_c$[e]	$^{16}O_c$[e]	t_L[f] $(\times 10^6$ yr)	$\log(L/L_\odot)$[g]	$\log(T_e)$[g]	$\log(L_H/L_\odot)$[h]
					$Z = 0.02$						
0.20..........	5.0	0.40	0.45	34	156.2	0.486	0.495	−1.80	2.805	3.674	2.51
0.20..........	4.0	0.28	0.36	75	297.5	0.312	0.669	−13.2	2.337	3.655	2.04
0.20..........	3.0	0.19	0.26	242	754.2	0.232	0.749	3.04	2.235	3.622	1.93
0.20..........	2.5	0.19	0.28	198	197.7	0.330	0.652	2.64	2.099	3.623	1.79
0.20..........	2.0	0.18	0.26	149	1519	0.264	0.718	−71.9	1.660	3.647	3.60
0.20..........	1.5	0.18	0.30	140	3900	0.256	0.734	−87.9	1.637	3.637	1.34
0.20..........	1.0	0.23	0.29	140	18840	0.289	0.685	−103	1.572	3.625	1.27
0.30..........	2.5	0.19	0.30	231	732.3	0.259	0.722	1.51	2.312	3.618	2.01
0.30..........	1.5	0.21	0.32	141	2151	0.274	0.710	1.30	2.318	3.596	2.01
					$Z = 0.01$						
0.20..........	2.5	0.19	0.28	301	1042	0.314	0.676	3.63	2.126	3.638	1.82
0.20..........	1.5	0.18	0.31	129	3119	0.276	0.716	−70.0	1.722	3.649	1.42
0.30..........	2.5	0.20	0.29	189	603.3	0.233	0.758	1.16	2.492	3.623	2.18
0.30..........	1.5	0.21	0.32	138	1768	0.213	0.780	1.81	2.466	3.602	2.15
					$Z = 0.001$						
0.20..........	3.0	0.24	0.39	80	408.3	0.520	0.479	0.151	2.683	3.657	2.37
0.20..........	2.5	0.25	0.41	152	702.4	0.306	0.693	0.379	2.490	3.661	2.16
0.20..........	2.0	0.21	0.37	125	1248	0.241	0.758	0.556	2.374	3.660	2.06
0.20..........	1.5	0.22	0.35	118	2756	0.268	0.731	−29.7	1.981	3.682	1.68
0.20..........	1.0	0.21	0.31	114	10154	0.333	0.666	−63.5	1.780	3.685	1.47
0.30..........	2.5	0.26	0.42	88	403.8	0.503	0.496	0.14	2.757	3.657	2.42
0.30..........	1.5	0.23	0.42	128	1659	0.198	0.801	0.62	2.551	3.650	2.24

[a] Maximum extent of the convective core.
[b] Maximum extent of the outer boundary of the semiconvective region.
[c] Time spent burning helium in the core.
[d] Time since ZAMS of core helium exhaustion.
[e] Central abundances following core helium exhaustion.
[f] Time since core helium exhaustion of equal L_H and L_{He}.
[g] Position in H-R diagram when $L_H = L_{He}$.
[h] Luminosity from hydrogen burning when $L_H = L_{He}$.

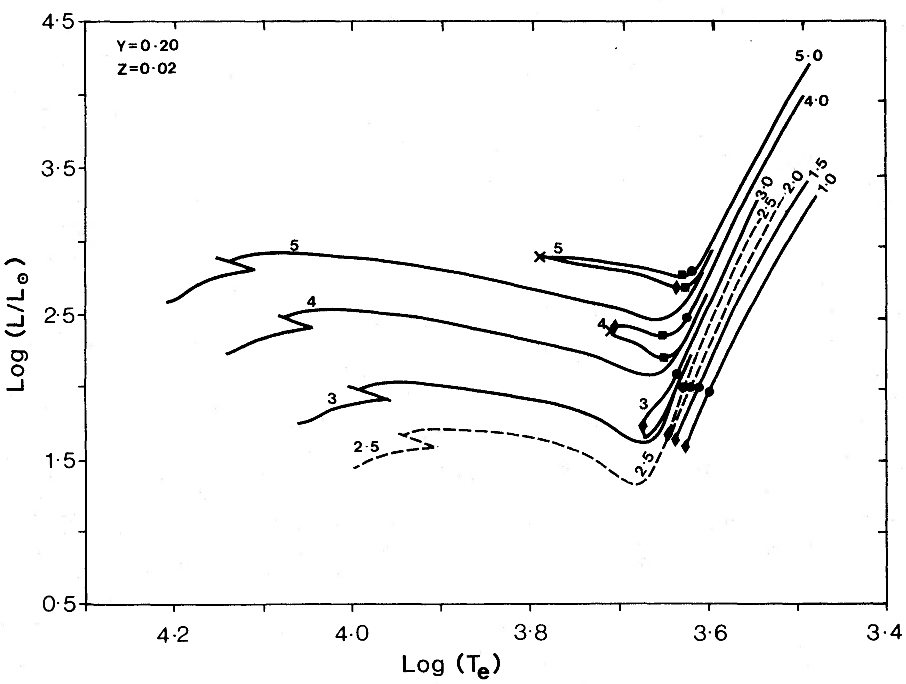

FIG. 1.—Evolutionary tracks for the $(Y, Z) = (0.20, 0.02)$ models with masses as indicated, in solar units. Tracks showing a blue loop have a cross marking the maximum blueward point of the loop and squares at the second and third red giant minima. All tracks have a diamond marking the point where $Y_c = 0.5$, and a filled circle indicates core helium exhaustion. Times to reach these evolutionary points are given in Table 4.

TABLE 3

ORDERED PAIRS OF [log ($L/L_\odot$), log (T_e)] FOR THE EVOLUTIONARY POINTS IN FIGURE 1

Y	$M/M_\odot$	RGM2[a]	$Y_c = 0.5$	Bluest Point Reached during Core He Burning	RGM3[a]	Core Helium Exhaustion
			$Z = 0.02$			
0.20..........	5.0	2.617, 3.627	2.643, 3.631	2.852, 3.790	2.748, 3.618	2.780, 3.615
0.20..........	4.0	2.197, 3.656	2.384, 3.711	2.377, 3.712	2.359, 3.661	2.434, 3.627
0.20..........	3.0	...	1.715, 3.676	...	...	2.150, 3.629
0.20..........	2.5	...	1.636, 3.666	...	...	2.138, 3.620
0.20..........	2.0	...	1.651, 3.647	...	...	2.017, 3.619
0.20..........	1.5	...	1.624, 3.636	...	...	2.022, 3.608
0.20..........	1.0	...	1.561, 3.626	...	...	1.954, 3.598
0.30..........	2.5	...	1.797, 3.660	...	...	2.195, 3.628
0.30..........	1.5	...	1.790, 3.635	...	...	2.237, 3.601
			$Z = 0.01$			
0.20..........	2.5	...	1.677, 3.678	...	...	1.966, 3.650
0.20..........	1.5	...	1.716, 3.648	...	...	2.065, 3.627
0.30..........	2.5	...	1.796, 4.075	...	...	2.360, 3.633
0.30..........	1.5	...	1.884, 3.650	...	...	2.340, 3.611
			$Z = 0.001$			
0.20..........	3.0	2.227, 3.685	2.576, 3.900	2.612, 3.904	2.547, 3.671	2.568, 3.665
0.20..........	2.5	1.876, 3.686	2.294, 3.819	2.367, 3.838	2.356, 3.748	2.366, 3.671
0.20..........	2.0	...	2.080, 3.717	2.127, 3.720	2.066, 3.690	2.351, 3.661
0.20..........	1.5	...	1.917, 3.696	...	...	2.173, 3.663
0.20..........	1.0	...	1.772, 3.684	...	...	2.056, 3.659
0.30..........	2.5	2.149, 3.687	2.594, 3.852	2.632, 3.853	2.702, 3.665	2.717, 3.660
0.30..........	1.5	...	2.093, 3.691	...	...	2.481, 3.654

[a] Second and third red giant minima.

TABLE 4

TIMES[a] TAKEN TO REACH THE LABELED POINTS IN FIGURE 1

Y	M ($M_\odot$)	RGM2[b]	$Y_c = 0.5$	Bluest Point Reached During Core He Burning	RGM3[b]	Core Helium Exhaustion
			$Z = 0.02$			
0.20..........	5.0	15.0	15.4	24.5	30.4	34
0.20..........	4.0	21.4	34.1	31.3	62.8	75
0.20..........	3.0	...	114	...	...	242
0.20..........	2.5	...	84	...	...	198
0.20..........	2.0	...	52	...	...	149
0.20..........	1.5	...	47	...	...	140
0.20..........	1.0	...	50	...	...	140
0.30..........	2.5	...	121	...	...	231
0.30..........	1.5	...	54	...	...	141
			$Z = 0.01$			
0.20..........	2.5	...	167	...	...	301
0.20..........	1.5	...	50	...	...	129
0.30..........	2.5	...	97	...	...	189
0.30..........	1.5	...	53	...	...	138
			$Z = 0.001$			
0.20..........	3.0	11	53	60	80	80
0.20..........	2.5	19	97	121	143	152
0.20..........	2.0	...	56	70	97	125
0.20..........	1.5	...	48	...	...	118
0.20..........	1.0	...	43	...	...	114
0.30..........	2.5	8.0	61	67	88	89
0.30..........	1.5	...	58	...	...	128

[a] Times in 10^6 yr since core helium ignition.
[b] Second and third red giant minima.

increases in importance relative to hydrogen burning as M decreases. That is, L_{He} first exceeds L_H progressively earlier in the evolution as M decreases. The same is true as Z increases, at constant M and Y, or as Y decreases, at constant M and Z. The maximum mass fraction in the convective core q_{cc}^{max} increases slightly as Y increases, at constant M and Z, or as Z decreases, for constant M and Y. The variation with total mass is more complex. Let M_F represent the upper mass limit for models which experience a helium core flash at a given Y and Z. Then q_{cc}^{max} increases as M decreases for $M < M_F$, and it decreases as M decreases for $M > M_F$. This reversal of behavior at $M \approx M_F$ was found to be quite common. It should be noted that the reason for q_{cc}^{max} increasing as M decreases (for $M < M_F$) is that the maximum mass of the convective core approaches a constant value, so the mass fraction increases as the total mass is decreased.

The time spent burning helium in the core t_{He} was found to peak at $M \approx M_F$, for a given abundance. This time decreases (slightly) as M decreases for $M < M_F$ or as M increases for $M > M_F$. Similarly, at a given Z, for $M < M_F$ we find t_{He} increases slightly as Y increases, but for $M > M_F$ we see that t_{He} decreases with increasing Y. The variation with Z is simpler, with t_{He} decreasing as Z decreases for a given M and Y.

d) The Luminosity and Temperature of the Clump Giants

During the core helium burning evolutionary stage of models with masses between ~ 1.0 and $2.5\ M_\odot$, the luminosity and effective temperature remain almost constant [log $(L/L_\odot)$ to within $\sim 5\%$ and log T_e to within $\lesssim 1\%$] for $\sim 70\%$ of the time spent burning helium in the core, and the model remains on the red giant branch. This is a higher mass extension of the horizontal branch. Such stars are called clump giants after the characteristic clump they produce in H-R diagrams and have been considered in detail by Cannon (1970).

The slight variation in position of the clump found from the current models may be fitted approximately by the following expressions:

$$\log (L/L_\odot) \approx 1.75 + 1.5(Y - 0.20) - 0.5 \log (Z/0.01) + 0.12(M/M_\odot - 1.5)\,,$$

$$\log T_e \approx 3.640 - 0.05(Y - 0.20) - 0.05 \log (Z/0.02) + 0.02\,(M/M_\odot)\,,$$

for Population I abundances, and

$$\log (L/L_\odot) \approx 1.90 + 0.4\,(M/M_\odot - 1.5) + 2(Y - 0.2)\,,$$

$$\log T_e \approx 3.680 + 0.04\,(M/M_\odot - 1.0)^2 - 0.03(Y - 0.20)\,,$$

for Population II abundances ($Z = 0.001$ being the only Z considered). The practical application of these formulae will be hindered by observational errors and the near constancy of L and T_e over a reasonable spread in mass and composition. Finally, we stress that these formulae were derived with $\alpha = l/H_p = 1.0$.

V. EVOLUTION THROUGH THE EARLY ASYMPTOTIC GIANT BRANCH PHASE

a) Definition and Comparison with Previous Calculations

The E-AGB evolution of stars with $3 \leq M/M_\odot \leq 11$ has been studied by Becker and Iben (1979, 1980, hereafter BI1 and BI2 respectively). I adopt the same terminology as far as possible, in an attempt to extend their results down to 1 $M_\odot$.

BI1 defined three types of E-AGB evolution, depending on the initial mass M_H^0 of the hydrogen-exhausted core:

Type I $\quad M_H^0 \gtrsim 1.1\ M_\odot$

Type II $\quad 0.8 \lesssim M_H^0/M_\odot \lesssim 1.1$

Type III $\quad M_H^0 \lesssim 0.8\ M_\odot$.

All the models discussed in this paper are of the third type except for the $(M, Y, Z) = (5.0, 0.20, 0.02)$ model, which was included primarily as a source of comparison between the BI models and those presented here. During E-AGB evolution the models pass through many distinct phases of evolution, as defined by BI1 and shown in Table 5. To the BI definitions we have added points 8′ and 10, which represent, respectively, the time of minimum luminosity from hydrogen burning reactions L_H and the time when the luminosity from helium burning L_{He} first exceeds L_H.

The case M model with $(M, Y, Z) = (5.0, 0.20, 0.02)$ may be compared with the equivalent BI1 model. We note, however, the following differences:

i) BI used $\alpha = l/H_p = 0.7$, and I used 1.0;

ii) BI used older opacities (Cox and Stewart 1970*a*, *b*);

iii) BI neglected semiconvection.

A detailed comparison between the BI model and that considered here showed very good agreement. The only differences worth noting are that the duration of the E-AGB lifetime (defined as the time elapsed between the last red giant minimum and the first thermal pulse) is $\sim 30\%$ shorter than found by BI, the model evolves at a slightly higher T_e (due to the different α used), and evolutionary points 5 and 7 occur in the opposite order. Comparison of the internal structure at the times of the maximum off-center temperature and the first thermal pulse showed very good agreement, and we may conclude that the present results will allow a smooth extension of the BI results to lower masses.

A comparison was also made between Gingold's (1975) model with $(M, Y, Z) = (2.0, 0.30, 0.02)$ and the 1.5 and 2.5 $M_\odot$

TABLE 5

DEFINITION OF EVOLUTIONARY STAGES DURING EARLY ASYMPTOTIC GIANT BRANCH EVOLUTION

Point	Description
E	Core helium exhaustion
L	Last red giant minimum
1	Negative luminosity profile first appears in the core
D	Start of second dredge-up phase
2	Maximum luminosity attained before shrinkage of hydrogen-exhausted core
3	Base of convective envelope first enters hydrogen-exhausted core
4	Maximum luminosity attained during second dredge-up episode
5	Helium burning shell reaches greatest strength
6	Maximum off-center temperature is reached (in the core)
7	Base of convective envelope begins to retreat outward in mass
8	Minimum luminosity attained during reignition of hydrogen burning shell
8′	Minimum luminosity of hydrogen burning shell
9	Maximum luminosity reached before first major thermal pulse
10	Energy output from helium burning first exceeds that of hydrogen burning

NOTE.—Most stages taken from BI.

models of the same abundances. In this case special attention was focused on the semiconvective regions, because Gingold used the Robertson and Faulkner method in these zones. The agreement in all aspects was good, with minor differences being entirely due to differences in input physics.

b) *Evolution of the Hydrogen-exhausted Core*

With the exception of the 5 $M_\odot$ model previously discussed, all the models constructed showed type III evolution, i.e., their initial $M_H^0 \lesssim 0.8\ M_\odot$ at core helium exhaustion and they do not pass through points D, 2, 3, 4, or 8 during their subsequent ascent of the giant branch. As an example of this evolution we discuss the case H, $(M, Y, Z) = (2.0, 0.20, 0.02)$ model. In this section we discuss the evolution of the hydrogen-exhausted core, and in the next we discuss the overall evolution.

Following core helium exhaustion the core contracts, reaching densities in the range 10^5–10^6 g cm^{-3}. These densities and temperatures ($\sim 10^8$ K) are conducive to large energy losses by neutrino emission, with these losses being a maximum in the center where the density is highest. When the cooling by neutrino losses exceeds the heating due to gravitational contraction, the center cools. The position of maximum temperature moves outward in mass, as shown in Figure 2, and a negative luminosity profile appears in the core as energy flows toward the center to make up for the neutrino loss. This is point 1, and it occurs 4×10^6 yr after core helium exhaustion.

Conditions within the core near point 1 are shown in Figure 3. Note that the maximum neutrino emission comes from the center. The off-center temperature maximum of 143×10^6 K is only slightly higher than the central temperature of 141×10^6 K. The peak in gravitational energy release occurs just interior to the helium burning shell, since the matter here is contracting rapidly as it "falls" onto the carbon-oxygen core. It is well known that helium burning in a shell favors production of ^{12}C rather than ^{16}O, and this is clearly seen in the ^{12}C profile in Figure 3. The discontinuity in the helium profile is at the position of the edge of the hydrogen-exhausted core at the time of the core flash, or $M = 0.465\ M_\odot$. Interior to this point we set $Y = 1.0 - Z - 0.03$, where the 0.03 allows for 3% helium burnt into carbon during the helium flash, as discussed earlier. Outside $M = 0.465\ M_\odot$, the helium abundance is $Y = 1.0 - Z$ as a result of processing by the hydrogen shell.

As the evolution continues, the off-center temperature maximum becomes more pronounced and moves outward in mass (see Fig. 2). The maximum off-center temperature is reached at point 6 and occurs some 12×10^6 yr after core helium exhaustion. Conditions within the core at this stage are shown in Figure 4. The maximum neutrino emission now occurs slightly outward from the center, and the integrated neutrino luminosity is $\sim 1\ L_\odot$. The maximum temperature of 163×10^6 K is significantly higher than the central temperature of 115×10^6 K. The helium burning shell has now burnt through the slight helium discontinuity left by the core flash, and seen in the previous figure. Note that the two nuclear shell sources are now separated by only $\sim 0.07\ M_\odot$, as opposed to $\sim 0.20\ M_\odot$ at point 1. Soon after point 6 the helium burning shell moves to within $\sim 0.04\ M_\odot$ of the hydrogen burning shell, and a thermal pulse follows.

Table 6 gives some selected properties of the various models at the time of the maximum off-center temperature (point 6). In agreement with BI2, I find that log $T^{\max}$ varies very linearly with the mass M_H' of the hydrogen-exhausted core at the time of the maximum temperature. An excellent fit to the results is

$$\log T^{\max} \approx 7.55 + 1.28(M_H'/M_\odot)\ . \quad (1)$$

For the masses considered, therefore, carbon burning is always negligible. The mass at the position of the maximum temperature is given quite accurately by

$$M(T^{\max})/M_\odot \approx 0.076 \exp(2.4M_H'/M_\odot)\ , \quad (2)$$

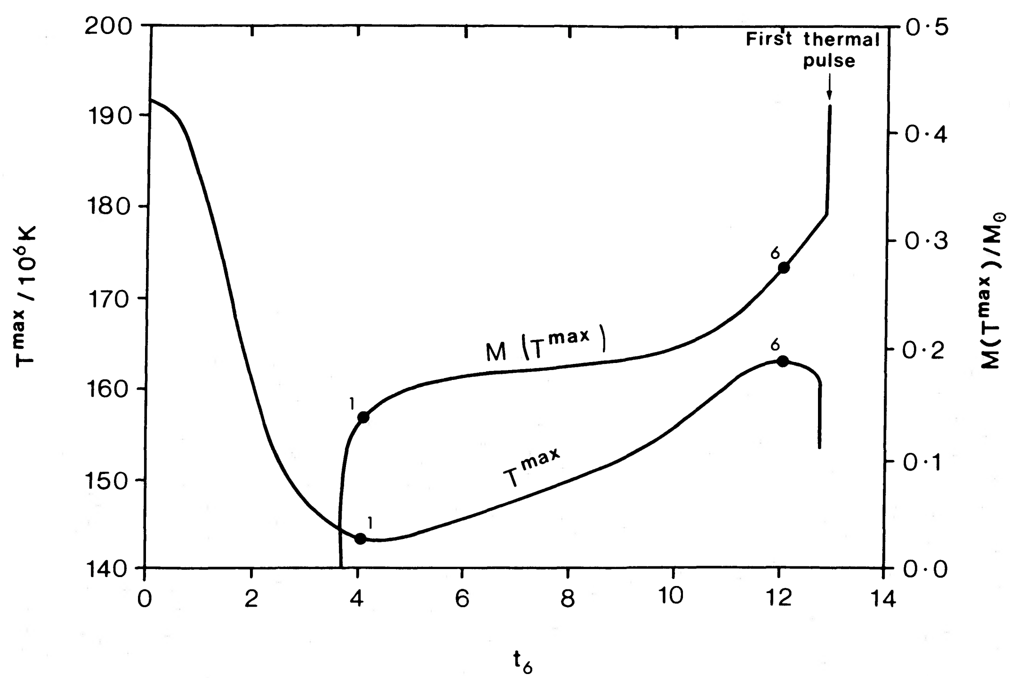

FIG. 2.—Variation of the maximum temperature and the mass at which it occurs, with time (in 10^6 yr) since core helium exhaustion for the model discussed in the text. Also shown are evolutionary points 1 and 6.

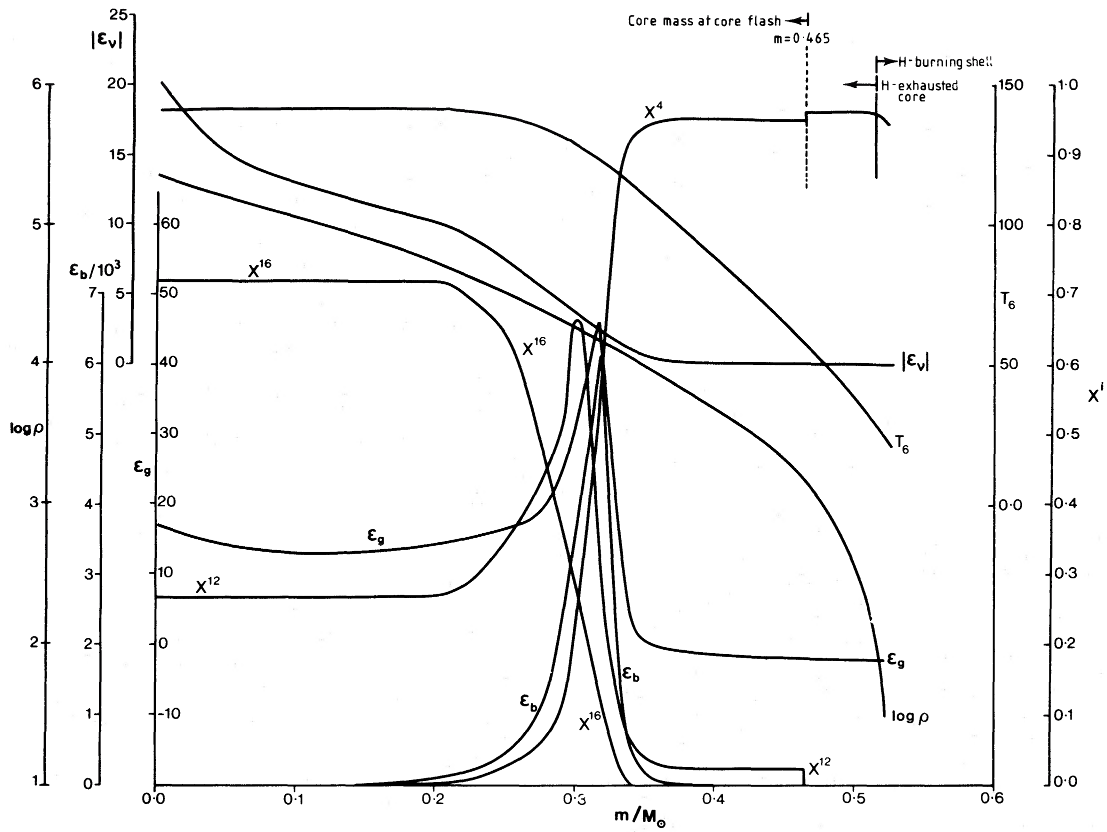

FIG. 3.—Conditions within the hydrogen-exhausted core at evolutionary point 1 for the model with $(M, Y, Z) = (2.0, 0.20, 0.02)$. Variable names and units are standard (e.g., T_6 is $T/10^6$ K; the various ϵ are in ergs g^{-1} s^{-1}; ϵ_b, ϵ_g, and ϵ_ν are the gravitational, nuclear burning, and neutrino energy generation rates respectively; note that ϵ_ν is negative).

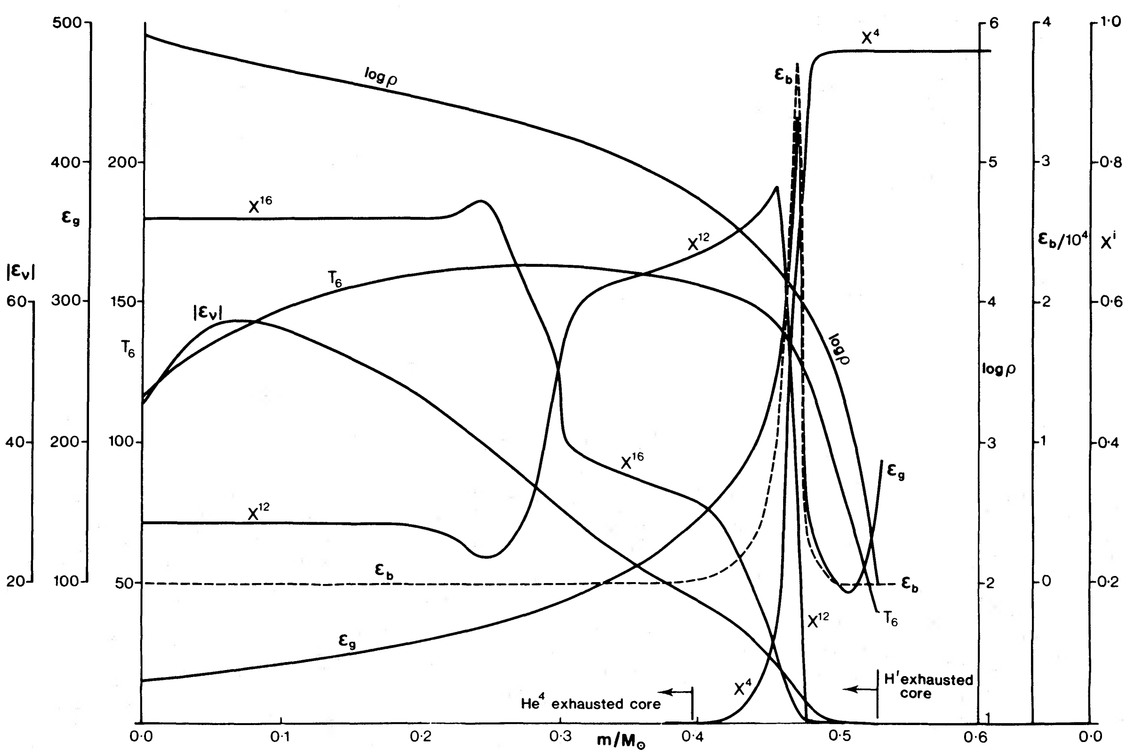

FIG. 4.—Same as Fig. 3, for evolutionary point 6

TABLE 6

CONDITIONS PREVAILING AT THE TIME OF MAXIMUM OFF-CENTER TEMPERATURE

Y	M ($M_\odot$)	t[a] (10^6 yr)	T^{max} (10^6 K)	$\rho(T^{max})$ (10^5 g cm^{-3})	$M(T^{max})$ ($M_\odot$)	M_H[b] ($M_\odot$)	M_{He}[c] ($M_\odot$)
			$Z = 0.02$				
0.20..........	5.0	1.856	382	6.41	0.602	0.864	0.841
0.20..........	4.0	3.270	280	4.58	0.415	0.709	0.653
0.20..........	3.0	10.973	165	2.03	0.276	0.528	0.395
0.20..........	2.5	16.970	154	1.50	0.310	0.510	0.382
0.20..........	2.0	11.984	163	1.97	0.272	0.524	0.389
0.20..........	1.5	11.555	166	2.04	0.271	0.529	0.396
0.20..........	1.0	13.514	161	1.77	0.272	0.519	0.376
0.30..........	2.5	10.267	177	2.43	0.287	0.552	0.434
0.30..........	1.5	9.119	183	2.59	0.290	0.561	0.456
			$Z = 0.01$				
0.20..........	2.5	17.017	153	1.43	0.298	0.505	0.355
0.20..........	1.5	9.734	171	2.24	0.276	0.539	0.412
0.30..........	2.5	5.538	207	3.28	0.303	0.599	0.509
0.30..........	1.5	6.266	198	3.02	0.299	0.585	0.490
			$Z = 0.001$				
0.20..........	3.0	3.313	306	4.70	0.480	0.750	0.707
0.20..........	2.5	4.148	244	3.99	0.361	0.656	0.593
0.20..........	2.0	5.307	209	3.29	0.306	0.601	0.516
0.20..........	1.5	7.064	187	2.77	0.282	0.566	0.462
0.20..........	1.0	9.193	173	2.35	0.271	0.542	0.421
0.30..........	2.5	3.260	324	4.19	0.513	0.746	0.740
0.30..........	1.5	4.046	232	4.09	0.329	0.640	0.570

[a] Times since core helium exhaustion.
[b] Mass of the hydrogen-exhausted core.
[c] Mass of the helium-exhausted core.

and, for $M'_H \lesssim 0.7$,

$$\log [\rho(T^{max})] \approx 4.04 \exp (0.52 M'_H/M_\odot) . \tag{3}$$

c) *To the First Thermal Pulse*

We begin by continuing the description of the (M, Y, Z) = (2.0, 0.20, 0.02) model. Following core helium exhaustion, the model moves to the base of the (second) giant branch. After a short rise, the luminosity briefly decreases and the model passes through the last red giant minimum. As noted by BI1, this corresponds to a maximum in energy absorption in the envelope. In the lower mass models considered here, however, this absorption is very small, being typically $\sim$5–10 $L_\odot$, compared with the surface luminosity of $\sim 300\,L_\odot$.

Figure 5 shows the time variation of L_H, L_{He}, and the total luminosity L since core helium exhaustion. The energy output of the hydrogen burning shell passes through a minimum (point 8′) with $\log (L_H^{min}/L_\odot) = 1.03$. In this respect the low-mass models again differ from those of BI1 who found that, for $M \gtrsim 3\ M_\odot$, the hydrogen burning shell was extinguished (the only exception was their type III model with $[M, Y, Z] = [3.0, 0.28, 0.01]$). We note, however, that in some cases (see Table 9 below) L_H^{min} is so low as to be effectively zero. But even in these cases there is no decrease in L as the hydrogen burning shell again grows in strength, and thus there is no point 8. Figure 5 shows the shallow peak in L_{He} (point 5) reached just before the first pulse.

The low energy generation of the hydrogen burning shell means that the mass of the hydrogen-exhausted core remains essentially fixed while the helium burning shell moves outward, as shown in Figure 6. This figure also shows the inward motion of the convective envelope and its final retreat (point 7) just before the flash. It is here that the models with $M \lesssim 3\ M_\odot$ exhibit another difference when compared to the more massive models. This is the fact that in none of the models considered here did the convective envelope penetrate the hydrogen-exhausted core before its retreat, in accord with equation (6) of BI1. Nevertheless, in most cases there is a small change in the surface abundances as the convective envelope reaches down to the top of the variable abundances profile of the hydrogen burning shell. The entropy gradient, due to the nonnegligible energy output of the shell, is sufficient to stop further penetration. This is discussed further in § V*d*.

In the majority of the models considered here, the evolutionary stages occur in the order 1, 8′, 5, 6, 7, 9, in agreement with the only example of type III evolution considered by BI1. Point 10, the point where L_{He} first exceeds L_H, occurs during core helium burning for the lower mass, solar metallicity models, but otherwise occurs very near the last red giant minimum.

In summary, then, the evolutionary behavior of all models is qualitatively similar, corroborating the expectation of BI1. Quantitative results for the evolutionary phases defined in Table 5 are given in Tables 7–9. No significant differences were found in test calculations which included the $^{14}N \rightarrow {}^{25}Mg$ reactions. The evolutionary tracks from core helium exhaustion to the first major thermal pulse are shown in Figures 7–12.

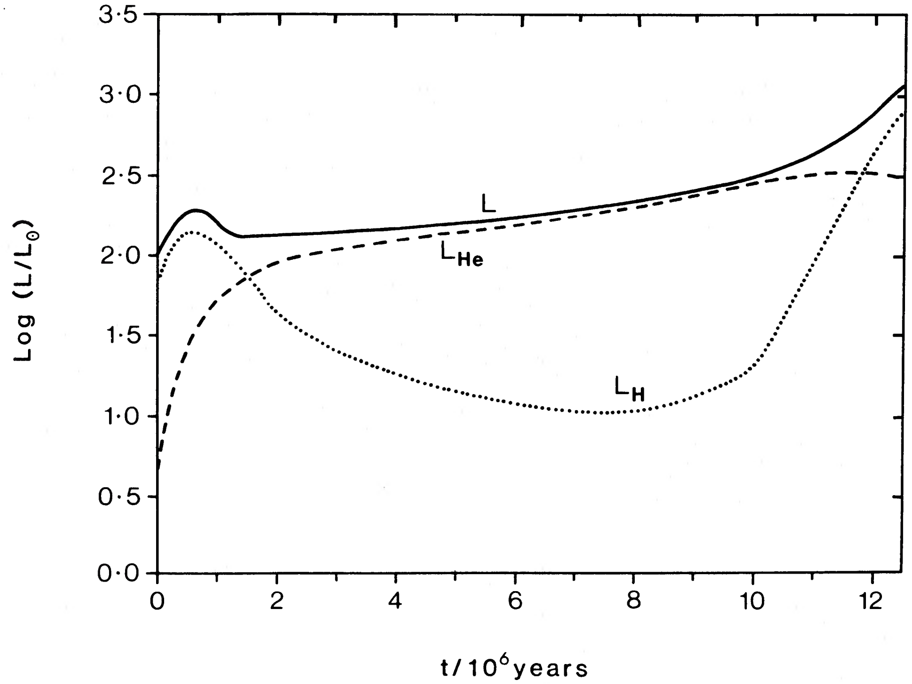

FIG. 5.—Variation of the various luminosities with time since core helium exhaustion for the $(M, Y, Z) = (2.0, 0.20, 0.02)$ sequence

During the E-AGB phase the evolutionary tracks are quite linear, and an excellent fit for the Population I compositions is

$$\log(L/L_\odot) \approx 3.268 - 11.8(\log T_e - 3.5) - 0.93 \log(Z/0.02) + 1.28 \log(M/1.5\ M_\odot) + 0.82 \log(Y/0.20) . \quad (4)$$

For $Z = 0.001$ we have

$$\log(L/L_\odot) \approx 3.170 - 16(\log T_e - 3.6) + 1.36 \log(M/1.5\ M_\odot) + 0.68 \log(Y/0.20) . \quad (5)$$

In both expressions recall that $\alpha = 1.0$ and $1.0 \leq M/M_\odot \leq 3.0$.

d) The "Almost" Second Dredge-Up

Only the case M, $(M, Y, Z) = (5.0, 0.20, 0.02)$ model experienced the second dredge-up, in accord with the results of BI1. It was found, however, that many of the models did show a small change in surface abundances because the maximum inward extent of the convective envelope at point 7 comes sufficiently close to the hydrogen burning shell to enter a region of varying abundance. This event will be called the "almost" second dredge-up, to distinguish it from the second dredge-up found in more massive stars, where the convective envelope actually penetrates the hydrogen exhausted core.

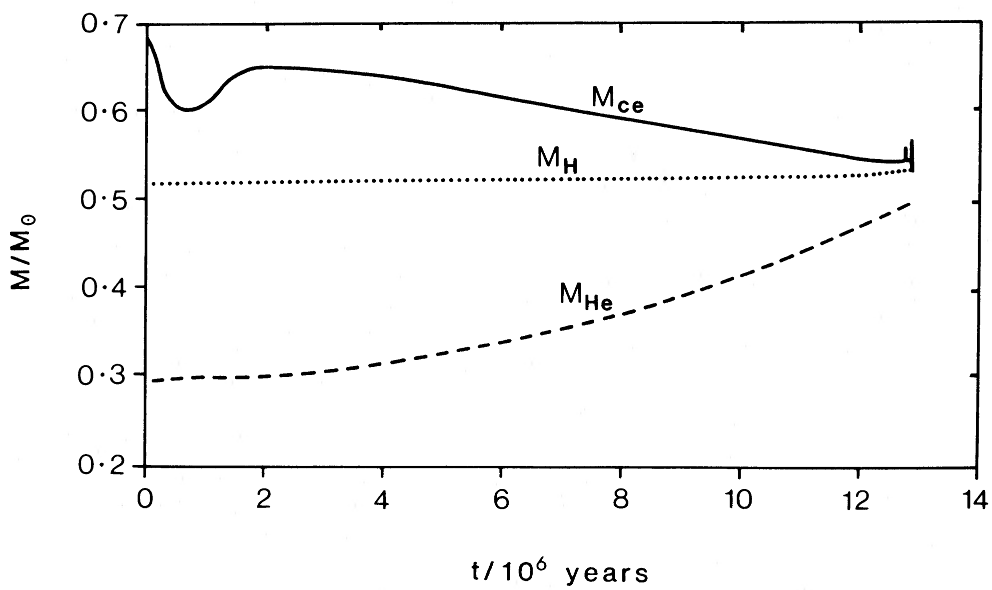

FIG. 6.—Time variation of the mass of the hydrogen exhausted core M_H, the mass at the center of the helium burning shell M_{He}, and the mass at the inner edge of the convective envelope M_{ce}. The horizontal axis is the time since core helium exhaustion.

TABLE 7

EVOLUTIONARY TIMES FOR THE POINTS DEFINED IN TABLE 5[a]

Y	$M/M_{\odot}$	EVOLUTIONARY STAGE E	L	1	5	6	7	8′	9	10
					$Z = 0.02$					
0.20	5.0	156.2	0.208	1.487	1.833	1.856	1.798	...	1.870	−1.800
0.20	4.0	297.5	0.572	2.161	3.171	3.270	3.250	2.818	3.340	−13.20
0.20	3.0	754.2	0.737	4.301	10.456	10.973	11.424	7.175	11.759	+3.040
0.20	2.5	197.7	4.080	4.940	15.745	16.976	17.021	10.060	17.642	+2.643
0.20	2.0	1519	3.175	4.075	11.654	11.984	12.418	8.275	12.724	−71.93
0.20	1.5	3900	2.818	4.677	11.018	11.555	11.921	8.342	12.439	−87.94
0.20	1.0	18840	1.730	5.065	13.101	13.514	13.950	9.513	14.548	−103.0
0.30	2.5	732.3	2.728	4.732	9.722	10.267	10.440	8.102	10.853	+1.514
0.30	1.5	2151	2.366	4.064	8.602	9.119	9.262	6.860	9.551	+1.304
					$Z = 0.01$					
0.20	2.5	1042	2.408	4.256	15.58	17.02	17.53	9.710	17.99	+3.632
0.20	1.5	3119	2.054	4.852	9.297	9.734	10.17	6.911	10.32	−70.01
0.30	2.5	603.3	1.569	3.246	5.186	5.538	5.647	4.351	5.764	+1.158
0.30	1.5	1768	2.351	3.337	5.855	6.266	6.361	4.676	6.566	+1.810
					$Z = 0.001$					
0.20	3.0	408.3	0.465	2.493	3.235	3.313	3.290	2.972	3.321	+0.151
0.20	2.5	702.4	0.724	2.653	3.920	4.148	4.253	3.281	4.258	+0.379
0.20	2.0	1248	0.440	3.107	5.010	5.307	5.438	4.029	5.487	+0.556
0.20	1.5	2756	1.135	3.467	6.547	7.064	7.319	4.854	7.317	−29.74
0.20	1.0	10154	1.612	3.709	8.604	9.193	9.686	6.132	9.690	−63.48
0.30	2.5	403.8	0.385	2.588	3.195	3.260	3.239	2.980	3.264	+0.144
0.30	1.5	1659	0.481	2.625	3.786	4.046	4.179	3.197	4.179	+0.618

[a] Time quoted for point E is the time since the ZAMS. For all other points the time is the time since point E. All times in 10^6 yr. For the 5 $M_{\odot}$ model, $t_D = 1.703$, $t_3 = 1.723$, and $t_8 = 1.852$.

TABLE 8

ORDERED PAIRS OF [$\log(L/L_{\odot})$, $\log(T_e)$] FOR EACH EVOLUTIONARY STAGE

Y	$M/M_{\odot}$	EVOLUTIONARY STAGE E	L	1	5	6	7	8′	9	10
					$Z = 0.02$					
0.20	5.0[a]	2.785, 3.613	2.870, 3.606	3.543, 3.548	4.172, 3.488	4.065, 3.498	4.085, 3.496	...	4.196, 3.484	2.805, 3.674
0.20	4.0	2.437, 3.626	2.554, 3.616	2.992, 3.580	3.645, 3.524	3.791, 3.510	3.755, 3.513	3.344, 3.551	3.937, 3.495	2.337, 3.655
0.20	3.0	2.071, 3.635	2.150, 3.629	2.213, 3.625	2.746, 3.583	2.913, 3.570	3.070, 3.557	2.351, 3.613	3.170, 3.549	2.235, 3.622
0.20	2.5	1.973, 3.633	2.081, 3.625	2.090, 3.624	2.660, 3.581	2.914, 3.561	2.921, 3.560	2.208, 3.615	3.095, 3.545	2.099, 3.623
0.20	2.0	2.011, 3.620	2.128, 3.611	2.152, 3.610	2.776, 3.560	2.878, 3.553	3.020, 3.540	2.338, 3.595	3.112, 3.532	1.660, 3.647
0.20	1.5	2.008, 3.607	2.133, 3.599	2.178, 3.596	2.722, 3.553	2.895, 3.537	3.017, 3.522	2.379, 3.580	3.280, 3.499	1.637, 3.637
0.20	1.0	1.946, 3.600	2.039, 3.591	2.118, 3.585	2.699, 3.537	2.831, 3.523	2.947, 3.511	2.300, 3.571	3.144, 3.492	1.572, 3.625
0.30	2.5	2.195, 3.628	2.285, 3.621	2.335, 3.616	2.893, 3.572	3.152, 3.550	3.242, 3.542	2.578, 3.597	3.453, 3.521	2.312, 3.618
0.30	1.5	2.237, 3.601	2.294, 3.597	2.344, 3.593	2.923, 3.545	3.197, 3.517	3.278, 3.509	2.578, 2.574	3.457, 3.490	2.318, 3.596
					$Z = 0.01$					
0.20	2.5	1.966, 3.650	2.119, 3.639	2.126, 3.638	2.570, 3.605	2.822, 3.587	2.923, 3.580	2.210, 3.632	3.018, 3.572	2.126, 3.638
0.20	1.5	2.065, 3.622	2.198, 3.613	2.300, 3.606	2.792, 3.568	2.943, 3.556	3.116, 3.539	2.447, 3.593	3.186, 3.534	1.722, 3.649
0.30	2.5	2.360, 3.633	2.469, 3.625	2.630, 3.612	3.088, 3.576	3.350, 3.554	3.448, 3.546	2.856, 3.594	3.578, 3.534	2.492, 3.623
0.30	1.5	2.340, 3.611	2.436, 3.606	2.527, 3.598	3.020, 3.558	3.295, 3.533	3.373, 3.526	2.729, 3.582	3.565, 3.506	2.466, 3.602
					$Z = 0.001$					
0.20	3.0	2.549, 3.672	2.638, 3.661	3.168, 3.627	3.807, 3.585	3.938, 3.576	3.910, 3.578	3.505, 3.605	3.941, 3.570	2.683, 3.657
0.20	2.5	2.366, 3.671	2.474, 3.662	2.852, 3.637	3.375, 3.606	3.581, 3.593	3.751, 3.580	3.064, 3.626	3.757, 3.580	2.490, 3.661
0.20	2.0	2.267, 3.667	2.373, 3.660	2.648, 3.643	3.118, 3.614	3.303, 3.603	3.385, 3.597	2.839, 3.632	3.443, 3.594	2.374, 3.660
0.20	1.5	2.164, 3.663	2.285, 3.656	2.550, 3.639	2.898, 3.617	3.103, 3.605	3.243, 3.595	2.594, 3.636	3.243, 3.595	1.981, 3.682
0.20	1.0	2.056, 3.659	2.201, 3.650	2.275, 3.644	2.272, 3.613	2.945, 3.602	3.204, 3.585	2.444, 3.634	3.205, 3.585	1.780, 3.685
0.30	2.5	2.717, 3.660	2.722, 3.661	3.255, 3.622	3.900, 3.578	4.035, 3.569	4.000, 3.571	3.592, 3.600	4.035, 3.568	2.757, 3.657
0.30	1.5	2.481, 3.654	2.548, 3.650	2.846, 3.630	3.275, 3.602	3.507, 3.586	3.704, 3.571	3.034, 3.618	3.704, 3.571	2.551, 3.650

[a] For the 5 $M_{\odot}$ model, point D occurs at (3.864, 5.518), point 3 at (3.907, 3.514), and point 8 at (3.987, 3.505).

TABLE 9

LUMINOSITIES DUE TO HYDROGEN AND HELIUM BURNING AT POINTS 5 AND 8′

Y	$M/M_\odot$	$\log(L_H^5/L_\odot)$	$\log(L_{He}^5/L_\odot)$	$\log(L_H^{8'}/L_\odot)$	$\log(L_{He}^{8'}/L_\odot)$
			$Z = 0.02$		
0.20..........	5.0	~ −10	4.108	...	...
0.20..........	4.0	1.902	3.594	−4.250	3.320
0.20..........	3.0	2.286	2.543	+1.073	2.351
0.20..........	2.5	2.326	2.366	+1.507	2.107
0.20..........	2.0	2.413	2.509	+1.029	2.309
0.20..........	1.5	2.193	2.550	+0.879	2.357
0.20..........	1.0	2.260	2.484	+1.072	2.267
0.30..........	2.5	2.375	2.714	+1.077	2.553
0.30..........	1.5	2.317	2.775	+0.758	2.560
			$Z = 0.01$		
0.20..........	2.5	2.164	2.341	+1.605	2.082
0.20..........	1.5	2.242	2.626	+0.751	2.429
0.30..........	2.5	1.928	3.029	−0.376	2.840
0.30..........	1.5	2.021	2.949	+0.172	2.715
			$Z = 0.001$		
0.20..........	3.0	2.450	3.739	−3.611	3.477
0.20..........	2.5	1.628	3.334	−1.655	3.047
0.20..........	2.0	2.032	3.052	−0.588	2.824
0.20..........	1.5	1.905	2.828	+0.206	2.582
0.20..........	1.0	2.095	2.649	+0.701	2.428
0.30..........	2.5	2.160	3.842	−4.021	3.562
0.30..........	1.5	1.946	3.221	−0.816	3.017

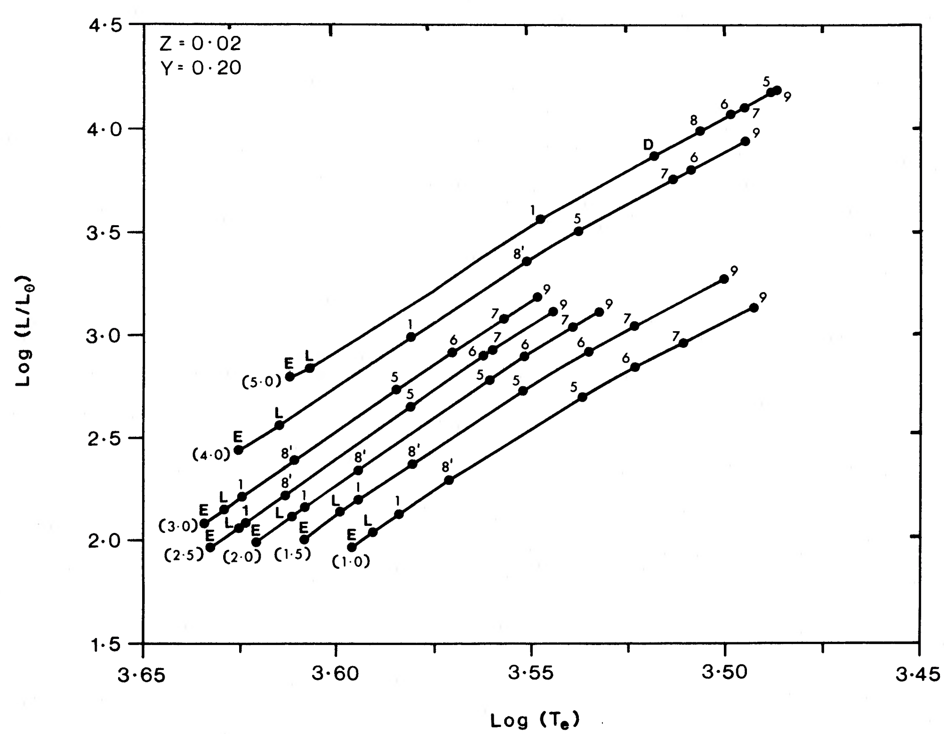

FIG. 7.—Evolutionary tracks from core helium exhaustion to the first major thermal pulse for the $(Y, Z) = (0.20, 0.02)$ models with masses as labeled (in solar units). Evolutionary points from Table 5 are shown.

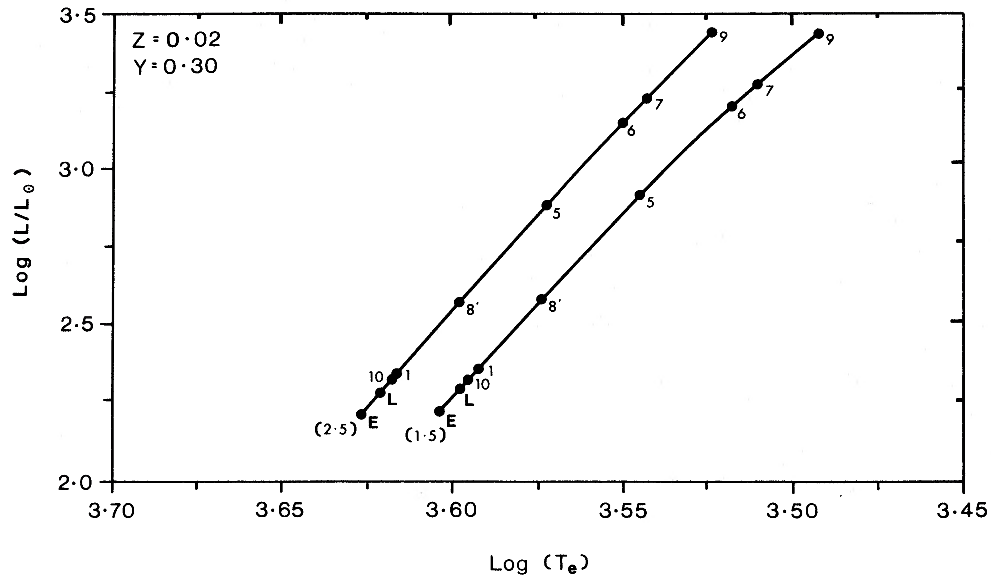

FIG. 8.—Same as Fig. 7, for $(Y, Z) = (0.30, 0.02)$

Table 10 shows some values of interest for each sequence. Note that of the $Z = 0.02$ models only the 4.0 $M_\odot$ show an "almost" second dredge-up, with lower mass models showing no change in their surface abundances, and models with $M \gtrsim 4$ $M_\odot$ experiencing the usual second dredge-up. Other entries in the table show that the "almost" second dredge-up can, for low Z ($\sim$0.001), lead to changes of $\sim$10%. The effect decreases with increasing Z at constant M and Y, or decreasing Y at constant M and Z. For $Z \gtrsim 0.01$ the "almost" second dredge-up can be safely neglected, as the surface abundance changes are typically $\lesssim$1%.

VI. EVOLUTION DURING THE THERMALLY PULSING ASYMPTOTIC GIANT BRANCH PHASE

a) The First Flash

Although the evolution of thermal pulses is well documented (see, for example, Gingold 1974; Iben 1975*a*, 1976, 1982; Fujimoto, Nomoto, and Sugimoto 1976; Sugimoto and Fujimoto 1978; Fujimoto and Sugimoto 1979; Sackmann 1977, 1980; Wood and Zarro 1981, hereafter WZ) we briefly discuss the first flash encountered in the $(M, Y, Z) = (2.0, 0.20, 0.02)$ sequence, thus completing the description of the evolution of

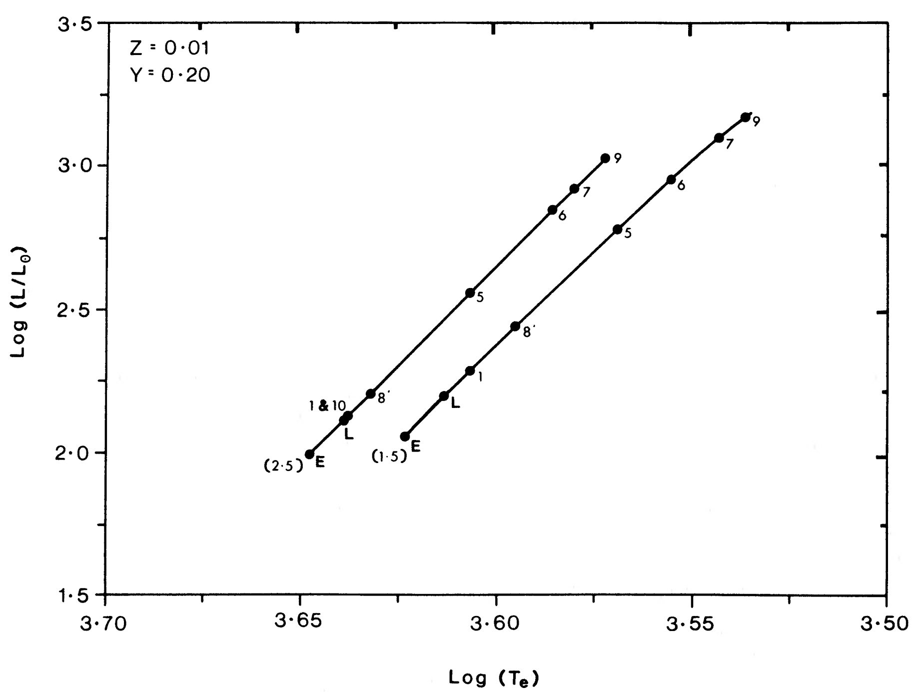

FIG. 9.—Same as Fig. 7, for $(Y, Z) = (0.20, 0.01)$

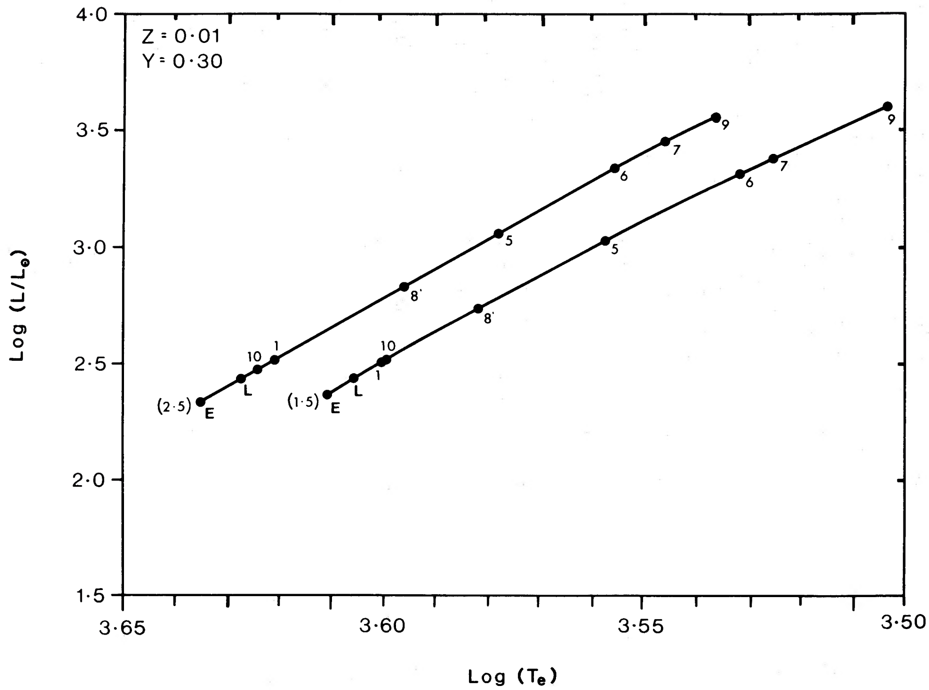

FIG. 10.—Same as Fig. 7, for $(Y, Z) = (0.30, 0.01)$

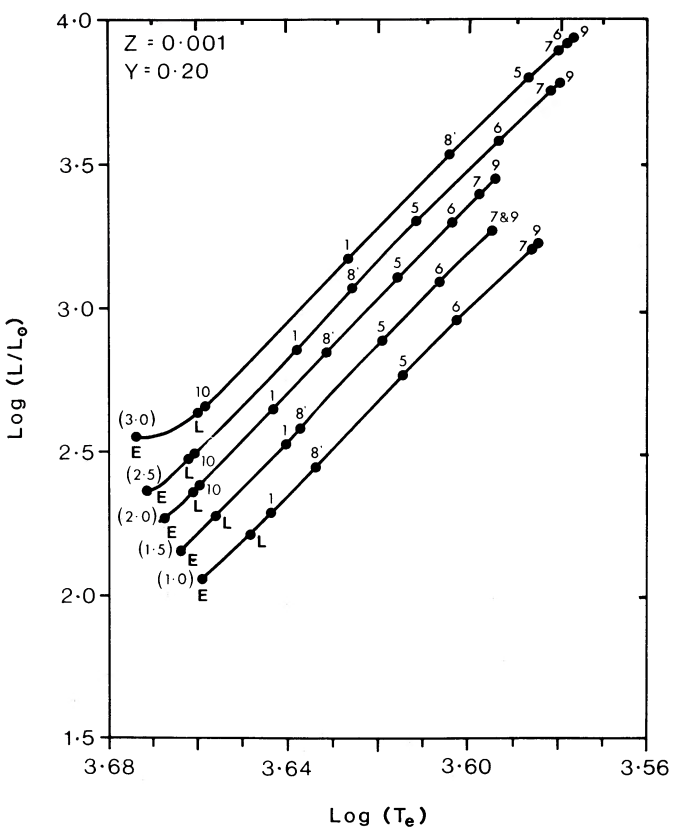

FIG. 11.—Same as Fig. 7, for $(Y, Z) = (0.20, 0.001)$

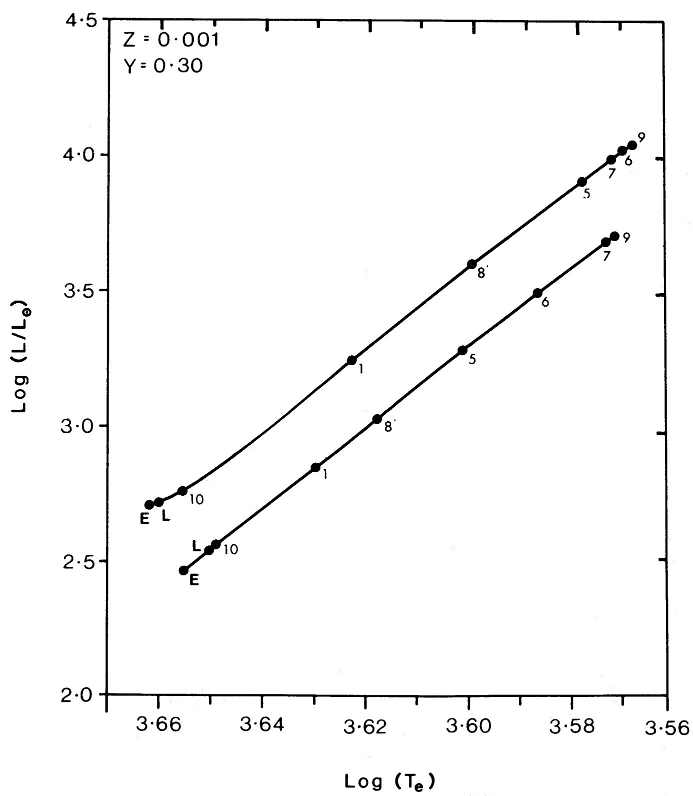

FIG. 12.—Same as Fig. 7, for $(Y, Z) = (0.30, 0.001)$

TABLE 10

ENVELOPE CONVECTION AND ITS CONSEQUENCES

Y	M ($M_\odot$)	M_{ce}^{7} [a] ($M_\odot$)	M_{H}^{7} [b] ($M_\odot$)	^{4}He [c]	^{12}C [c]	^{14}N [c]	^{16}O [c]
			$Z = 0.02$				
0.20..........	5.0	0.864	0.864	1.027	0.977	1.045	0.992
0.20..........	4.0	0.713	0.708	1.000	0.990	1.009	1.000
0.20..........	3.0	0.544	0.532	1.000	1.000	1.000	1.000
0.20..........	2.5	0.525	0.511	1.000	1.000	1.000	1.000
0.20..........	2.0	0.540	0.528	1.000	1.000	1.000	1.000
0.20..........	1.5	0.544	0.532	1.000	1.000	1.000	1.000
0.20..........	1.0	0.535	0.522	1.000	1.000	1.000	1.000
0.30..........	2.5	0.566	0.555	1.000	1.000	1.000	1.000
0.30..........	1.5	0.574	0.564	1.000	1.000	1.000	1.000
			$Z = 0.01$				
0.20..........	2.5	0.526	0.508	1.000	1.000	1.000	1.000
0.20..........	1.5	0.555	0.543	1.000	1.000	1.006	1.000
0.30..........	2.5	0.612	0.602	1.000	0.993	1.006	1.000
0.30..........	1.5	0.598	0.587	1.000	0.990	1.013	1.000
			$Z = 0.001$				
0.20..........	3.0	0.755	0.749	1.019	0.827	1.257	0.964
0.20..........	2.5	0.665	0.661	1.001	0.974	1.040	0.995
0.20..........	2.0	0.617	0.605	1.001	0.969	1.034	0.997
0.20..........	1.5	0.585	0.570	1.003	0.963	1.045	1.000
0.20..........	1.0	0.560	0.547	1.001	0.938	1.145	1.000
0.30..........	2.5	0.779	0.775	1.008	0.850	1.258	0.987
0.30..........	1.5	0.639	0.646	1.000	0.947	1.061	0.998

[a] Mass at base of convective envelope at its maximum inward penetration (point 7).

[b] Mass of hydrogen-exhausted core at point 7.

[c] Enhancement ratio for the new surface abundances, in the sense (abundance after "almost"-second dredge-up)/(abundance after first dredge-up). The only exception is the 5 $M_\odot$ model, which shows a normal second dredge-up.

this model and introducing the notation to be used. The dependence of the results on mass and composition is then given.

Once the hydrogen- and helium-exhausted cores move to within $\sim 0.10\ M_\odot$ of each other, or the (centers of the) nuclear burning shells are separated by only $\sim 0.05\ M_\odot$, the energy output of the helium burning shell begins to oscillate. These values are nearly independent of mass and composition. In the $(M, Y, Z) = (2.0, 0.20, 0.02)$ sequence the two oscillations found prior to the first major thermal pulse (also known as minipulses) show an amplitude of only ~ 0.02 in log $(L_{\rm He}/L_\odot)$. This was typical of many of the models considered.

At the time of the first major pulse, defined as the first pulse of sufficient strength to drive a convective shell (also known as the intershell convective zone) just outside the helium burning shell, the hydrogen-exhausted core contains $M_{\rm H} = 0.531\ M_\odot$ and the carbon-oxygen core contains $M_{\rm He} = 0.423\ M_\odot$. The hydrogen burning shell is very thin ($\sim 0.001\ M_\odot$) and may be considered to be centered at the edge of the hydrogen-exhausted core. The helium burning shell, however, is of not insignificant width, being centered on $M = 0.490\ M_\odot$.

During the first major thermal pulse, the luminosity from helium burning reactions rises to a maximum of log $(L_{\rm He}^{\rm max}/L_\odot) = 3.8$, and in the ensuing expansion of the outer layers the hydrogen burning shell is essentially extinguished, its output dropping to $\sim 1\ L_\odot$. The helium burning shell cannot remove sufficiently rapidly all the energy deposited by the triple-α reactions, and its temperature rises by a factor of ~ 1.4 to $\sim 178 \times 10^6$ K. The maximum temperature in the star is no longer found in the carbon-oxygen core but now occurs at the base of the helium burning shell, although the density in the shell center drops by a factor of ~ 3 to ~ 3200 g cm^{-3}. A temperature inversion now occurs at the base of the helium burning shell. The temperature difference is $\sim 50 \times 10^6$ K, and the peak has a temperature $\sim 178 \times 10^6$ K. This inversion drives a negative luminosity profile just below the shell, with a minimum luminosity of $\sim -4\ L_\odot$.

During the pulse the carbon-oxygen core expands slightly and the central density drops from $\sim 1.1 \times 10^6$ g cm^{-3} to $\sim 1.0 \times 10^6$ g cm^{-3}. Simultaneously the central temperature drops by 4% to $\sim 100 \times 10^6$ K.

The high-energy output of the thermal runaway in the helium burning shell drives a convective zone beginning just above the center of the helium burning shell. At its maximum extent the convective shell covers $\Delta M_{\rm cs}^{\rm max} = 0.021\ M_\odot$ and reaches to within 0.024 $M_\odot$ of the hydrogen-rich envelope. During the following interpulse phase the convective envelope reaches down to $M = 0.539\ M_\odot$ and falls 0.007 $M_\odot$ short of reaching into the hydrogen-exhausted core and 0.024 $M_\odot$ short of the carbon-rich shell.

The time elapsed between the last minipulse and the first major thermal pulse is $P = 7.7 \times 10^4$ yr. This is within a factor of 2 of the value predicted by the Paczyński (1975) relation

$$\log P \approx 3.05\text{–}4.5(M_{\rm H}/M_\odot - 1.0)\ . \qquad (6)$$

The three main core mass–luminosity relations are

$$L_P/L_\odot \approx 59{,}250(M_{\rm H}/M_\odot - 0.522)\ , \qquad (7)$$

due to Paczyński (1970),

$$L_{\rm I}/L_\odot \approx 6.34 \times 10^4(M_{\rm H}/M_\odot - 0.44)(M/7\ M_\odot)^{0.4}\ , \qquad (8)$$

due to Iben (1977), and

$$L_{\rm WZ}/L_\odot \approx 59{,}250(M_{\rm H}/M_\odot - 0.495)\ , \qquad (9)$$

due to WZ. For the model under consideration we find $L_P = 550\ L_\odot$, $L_{\rm I} = 1290\ L_\odot$, and $L_{\rm WZ} = 2133\ L_\odot$. Obviously we would expect the Paczyński relation to fail as $M_{\rm H} \rightarrow 0.522\ M_\odot$. Iben's expression was derived from much larger core masses and is not directly applicable to our case. Similarly, the WZ expression, although relevant to the low-mass and low–core mass stars, was (like the others) derived from full-amplitude calculations and thus overestimates the luminosity prior to the first pulse.

Figure 13 shows the various nuclear luminosity sources during the first two pulses. The first cycle shows no substantial minipulses following the major pulse, although they are seen after the second pulse (see Schwarzschild and Härm 1967 for a discussion of multiple pulses). In agreement with other authors (e.g., Gingold 1974; WZ; Iben 1982) we find that for $\sim 20\%$ of the interpulse phase following a pulse (in this case the first), the surface luminosity is at least 0.5 mag below the prepulse maximum. Such variation in the luminosity during a pulse cycle has important ramifications for our understanding of C-star luminosities (e.g., Iben 1982).

Table 11 gives various values relevant to all sequences at the time of the first major pulse. Figure 14 shows the variation with mass of the mass of the hydrogen-exhausted core at the time of the first pulse, $M_{\rm H}(1)$, for each composition considered. By combining with the results of BI2 we now have $M_{\rm H}(1)$ as a function of mass between 1.0 and 7.0 $M_\odot$ for $Z = 0.02$ and

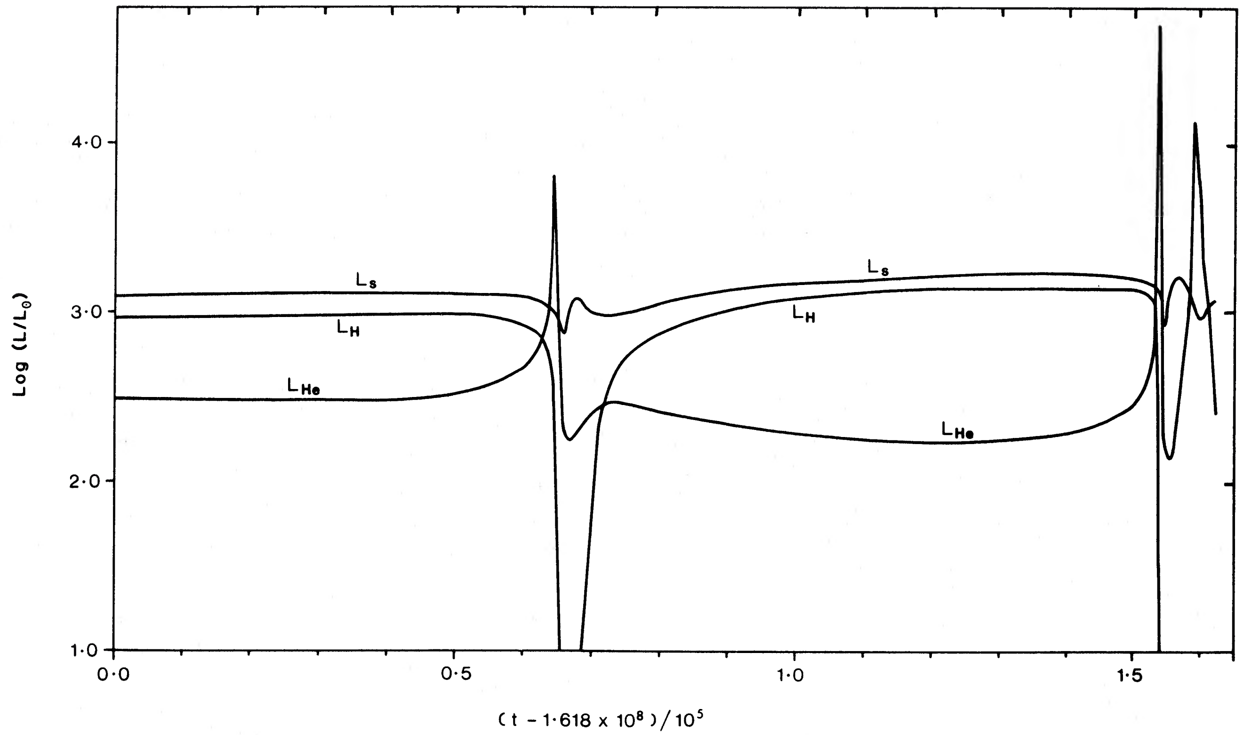

FIG. 13.—Time variation of luminosity sources during the first two pulses of the sequence for $(M, Y, Z) = (2.0, 0.20, 0.02)$

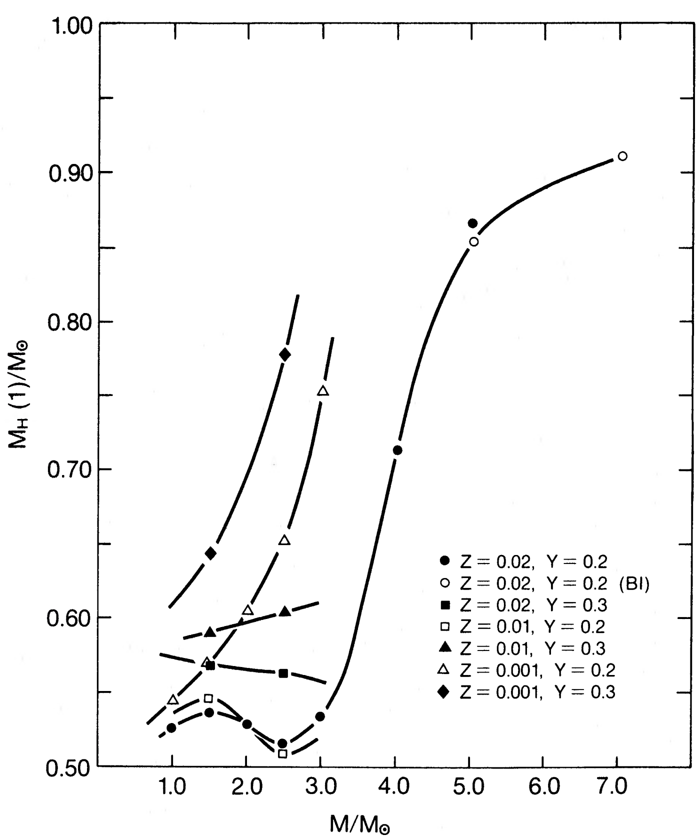

FIG. 14.—Variation, with total stellar mass, of the mass of the hydrogen-exhausted core at the first major thermal pulse. Note that the values of $M_H(1)$ for the $(M, Y, Z) = (1.5, 0.20, 0.001)$ and $(1.5, 0.30, 0.02)$ sequences are essentially equal.

TABLE 11

MODEL DETAILS AT THE FIRST FLASH

Y	M ($M_\odot$)	M_H[a] ($M_\odot$)	M_{He}[b] ($M_\odot$)	P[c] (10^4 yr)	$\log(L_{He}^{max})$[d] ($L_\odot$)	ΔM_{cs}^{max}[e] ($M_\odot$)	N[f]
			$Z = 0.02$				
0.20	5.0	0.867	0.847	0.50	5.025	0.004	2
0.20	4.0	0.715	0.675	1.7	5.329	0.012	2
0.20	3.0	0.536	0.432	6.9	4.079	0.027	6
0.20	2.5	0.517	0.397	8.9	4.366	0.038	5
0.20	2.0	0.531	0.423	7.7	3.807	0.021	2
0.20	1.5	0.538	0.434	8.0	4.830	0.035	3
0.20	1.0	0.528	0.419	7.8	4.658	0.037	4
0.30	2.5	0.565	0.472	4.5	4.298	0.023	4
0.30	1.5	0.572	0.485	3.9	4.275	0.022	2
			$Z = 0.01$				
0.20	2.5	0.513	0.391	9.7	4.112	0.034	5
0.20	1.5	0.545	0.447	6.5	4.048	0.025	3
0.30	2.5	0.606	0.534	2.8	4.287	0.017	2
0.30	1.5	0.593	0.515	3.6	4.704	0.023	4
			$Z = 0.001$				
0.20	3.0	0.754	0.723	...	4.975	0.008	0
0.20	2.5	0.662	0.609	3.3	5.475	0.017	1
0.20	2.0	0.606	0.533	3.5	4.356	0.018	1
0.20	1.5	0.570	0.484	4.2	4.231	0.019	2
0.20	1.0	0.547	0.442	8.2	4.750	0.033	3
0.30	2.5	0.780	0.748	0.73	4.450	0.005	1
0.30	1.5	0.646	0.589	2.9	5.040	0.017	2

[a] Mass of hydrogen-exhausted core.
[b] Mass of the helium-exhausted core.
[c] Time between the last minipulse and the first major pulse.
[d] Maximum luminosity from helium burning.
[e] Maximum extent of convective shell.
[f] Number of minipulses prior to the first major pulse.

$Y = 0.20$. We note that $M_H(1)$ possesses a minimum at $M \approx M_F$ for Population I compositions. There is then a slight oscillation of $M_H(1)$ as M decreases, but the amplitude is small and may be ignored. For Population I abundances we thus have

$$M_H(1)/M_\odot \approx 0.53 - (1.3 + \log Z)(Y - 0.20)\,, \quad (10)$$

and for Population II compositions ($Z = 0.001$) we have

$$M_H(1)/M_\odot \approx (0.394 + 0.3Y)\exp[(0.10 + 0.3Y)M/M_\odot]\,. \quad (11)$$

Perhaps the most noticeable features are the relative constancy of $M_H(1)$ for $M < M_F$ and Population I abundances, and the very strong dependence of $M_H(1)$ on M for the low-metallicity models. Note also that an increase in Y from 0.20 to 0.30 can increase $M_H(1)$ by $\sim 0.05\ M_\odot$ for Population I models, and by $\sim 0.10\ M_\odot$ for Population II models.

The time P in years between the last minipulse and the first major pulse is found to obey

$$\log P \approx 7.0 - 4.0 M_H/M_\odot\,. \quad (12)$$

The luminosity maximum just prior to the first pulse is given by

$$L/L_\odot \approx 41{,}000(M_H/M_\odot - 0.5)\,, \quad (13)$$

for Population I abundances, and by

$$L/L_\odot \approx 36{,}700(M_H/M_\odot - 0.515)\,, \quad (14)$$

for Population II abundances.

b) Full Amplitude Calculations

After the first thermal pulse, successive pulses are initially separated by an increasing time. During this period of evolution the maximum quiescent surface luminosity (just before a pulse) and the maximum luminosity of the helium burning shell (during a pulse) increase with each successive pulse. After $\sim$5–10 pulses these increases become much slower, and we say the pulses have reached full amplitude (e.g., Gingold 1974, 1975; Sackmann 1980; Iben 1976, 1982; WZ). Each of the 1.5 $M_\odot$ models has been evolved through to full amplitude of the thermal pulses. It is proposed to continue the evolution of the other masses also, but we present here only the results for the 1.5 $M_\odot$ models.

Once full amplitude has been reached, the period P between pulses begins to decrease almost linearly with M_H (e.g., Paczyński 1970; WZ). The maximum quiescent luminosity also increases almost linearly with mass (Paczyński 1970; Iben 1977; Havazelet and Barkat 1979; Kippenhahn 1981; Tuchman, Glasner, and Barkat 1983; WZ). With successive pulses the outer edge of the intershell convective zone reaches progressively closer to the hydrogen-rich envelope. Simultaneously the maximum inward penetration of the convective envelope during the interpulse phase increases and reaches successively close to the hydrogen-exhausted core and the carbon-enriched intershell region. In none of the calculations during the TP-AGB phase of the 1.5 $M_\odot$ models did either of these convective zones penetrate the hydrogen-helium interface, and thus in no case were the nucleosynthetic products mixed to the surface (but see § VII).

From these calculations of full-amplitude pulses we can derive a linear relation between the mass M_H of the hydrogen-exhausted core (actually the center of the hydrogen burning shell) and the maximum prepulse quiescent luminosity. The results showed a fairly substantial dependence on Y, with the gradient increasing as Y is increased. The zero point of the relation was also found to depend on Y and, to a lesser extent, Z. An excellent fit for Population I abundances is given by

$$L_Q/L_\odot \approx 55{,}320[2.3(Y - 0.20) + 1.0](M_H/M_\odot - a)\,, \quad (15)$$

where

$$a = 0.489 + 0.23(Y - 0.20) - 0.70(Z - 0.02)\,. \quad (16)$$

Neglecting the abundance dependence yields the less accurate formula

$$L_Q/L_\odot \approx 56{,}730(M_H/M_\odot - 0.495)\,, \quad (17)$$

which is in reasonable agreement with the expression derived by WZ (eq. [9]). For the $Z = 0.001$ calculations we find

$$L_Q/L_\odot \approx 51{,}800[1.0 + 4.7(Y - 0.20)]M_H/M_\odot - 26{,}260 \times [1.0 + 6.2(Y - 0.20)]\,. \quad (18)$$

The relationship between the core mass and the interpulse period P for the Population I models is

$$\log P \approx 2.31(2.74 - M_H/M_\odot)\,. \quad (19)$$

The gradient in this expression is considerably less than found by WZ. This is most likely due to the newer opacity tables used in the present calculations (and possibly the inclusion of semiconvection), because the evolutionary code used is essentially the same. Note also that the expression derived by WZ covers a much larger range in M_H up to $\sim 0.9\ M_\odot$. For the Population II compositions considered here ($Z = 0.001$), we find a not insignificant Y-dependence, and an approximate relation is

$$\log P \approx 3.67[1.0 - 2.3(Y - 0.20)] \times [2.0 + 3.4(Y - 0.20) - M_{\rm H}/M_\odot] \ . \quad (20)$$

c) *Inclusion of Low-Temperature Opacity*

After the previously discussed calculations were completed, D. Alexander (private communication) kindly provided opacity tables for the range $T \leq 10^4$ K. The opacities provided were generated in the manner outlined in Alexander (1975) and include the effects of both molecular and grain opacity sources. The former, being calculated by straight means, are thought to represent an upper limit (Alexander, Johnson, and Rympa 1983). The resulting opacity values can be up to four orders of magnitude larger than the Cox and Stewart (1970*b*) tables for $\log T \lesssim 3.5$. To determine the effect of these opacities on the evolution we recalculated the entire evolution of the (M, Y, Z) = (1.5, 0.20, 0.02) model from the ZAMS (this is a case F model). The evolution prior to the giant branch was, as expected, almost identical. The ascent of the giant branch occurred some 0.03 cooler in $\log T_e$, again as expected. Evolution during the core helium burning phase was again virtually identical, and the surface abundance change through the first and "almost" second dredge-up agreed to within 3%. The evolutionary tracks began to diverge as the model ascended the second giant branch. Interior conditions and the various E-AGB phases are unchanged by the new opacity, except for the significantly cooler stellar surface (up to 0.05 in $\log T_e$). The evolution was followed through 19 thermal pulses, and with the exception of the cooler surface temperature, the differences were totally negligible.

We note here the recent evolutionary calculations of VandenBerg, which also use the Huebner *et al.* (1977) opacities for $T > 10^4$ K and those of Alexander (1975) for $T < 10^4$ K. By using model atmospheres to provide realistic boundary conditions, VandenBerg and co-workers have found very good agreement with the observations (see VandenBerg 1983, 1985; VandenBerg *et al.* 1983; VandenBerg and Bell 1985; Fahlman, Richer, and VandenBerg 1985; VandenBerg and Bridges 1984; VandenBerg and Hrivnak 1985). Note that as a result of these extensive comparisons, VandenBerg strongly favors $\alpha \approx 1.5$. It should be remembered, however, that there is no reason to deny the possibility that α varies with depth in a star (e.g., Demarque, King, and Diaz 1982), or with the various phases of evolution.

VII. CONSEQUENCES AND APPLICATIONS

It is well known that calculations of synthetic AGB populations (e.g., Wood and Cahn 1977; Iben and Truran 1978; Iben 1981; Renzini and Voli 1981) fail to produce C stars at the low luminosities demanded by the observations (e.g., Gingold 1975; Frogel, Persson, and Cohen 1980; Mould and Aaronson 1980; Richer 1981) and produce too many C stars at high luminosities.

This latter problem has many important consequences (e.g., Iben 1984). Various solutions have been proposed (Iben 1981) but none have been entirely satisfactory (e.g., Becker 1982). More recently it has been suggested that convective overshooting and the helium spike phenomenon may act to increase the mass of the carbon-oxygen core when the core helium supply is finally consumed (Renzini *et al.* 1985; Castellani *et al.* 1985*a*, *b*). This would have the effect of lowering the maximum mass star $M_{\rm up}$, which develops a degenerate carbon-oxygen core. Stars with $M > M_{\rm up}$, which ignite carbon gently, avoid the AGB phase. So lowering $M_{\rm up}$ lowers the maximum mass found on the AGB and thus lowers the maximum luminosity of C stars found on the AGB, in accord with the observations. A similar effect can result from convective overshooting (C. Chiosi, private communication). We note that the 5 $M_\odot$ model considered in this paper has a carbon-oxygen core mass of $\sim 0.57\ M_\odot$ at the time of core helium exhaustion, whereas in the BI model (same abundances, but semiconvection neglected) at this time the core mass was only 0.318 $M_\odot$. This change is in the direction required, although further calculations are necessary before definite conclusions can be reached (see Castellani *et al.* 1985*a*, *b*).

The discrepancy at low luminosities, which concerns the calculations presented here, is due to the fact that theoretical models of low-luminosity (= low $M_{\rm H}$ = low M) stars fail to dredge carbon to their surfaces for values of $M_{\rm H}$ as low as is thought necessary. Analysis of photometric data for C stars in the Magellanic Clouds by various authors (e.g., Richer 1981; Scalo and Miller 1981; Miller and Scalo 1982) demands that dredge-up begin, in Magellanic Cloud C stars, with essentially the first pulse. Wood (1981) has found dredge-up of carbon for $M_{\rm H} \approx 0.67\ M_\odot$ in studies of a 2 $M_\odot$ model, with (Y, Z) = (0.25, 0.001). This model became a C star when $M_{\rm H}$ reached 0.698 $M_\odot$. The lowest core mass for which the third dredge-up has been found to operate is $M_{\rm H} \approx 0.61\ M_\odot$ in the calculations of Iben and Renzini (1982*a*, *b*) for a 0.7 $M_\odot$, (Y, Z) = (0.25, 0.001) model with $\alpha = 1.5$. In these calculations a semiconvective zone forms which diffuses carbon outward and hydrogen inward. Iben and Renzini found that C-star characteristics were obtained after very few pulses, no doubt partly due to the low envelope mass ($\sim 0.09\ M_\odot$) in which the carbon-rich material was diluted. There is some debate, however, concerning the applicability of this mechanism to stars of different masses. Indeed, P. Wood (private communication) has been unable to reproduce the results of Iben and Renzini (1982*a*, *b*). See also Hollowell (1986). It was suggested by Iben and Renzini (1983) that this may be due to Wood's use of time steps that were too large, but further calculations by Wood indicated that this was not the case. More recently, Iben and Renzini (1984) have identified the fact that they find $L_{\rm He}^{\rm max}$ to be about an order of magnitude larger than found by Wood. The reason for this difference is unknown at present. We conclude that although Iben and Renzini have sounded timely warnings concerning input physics, the details of the "Iben-Renzini" mechanism are not yet well established. The strange "on-off" behavior suggested by Iben and Renzini (1984) must be further investigated, and until there is consensus on the details of this mechanism it may be a little early to claim that the problem of the existence of low-luminosity C stars is solved. In any case, it is unclear whether this mechanism can operate in more massive stars ($\sim 2\ M_\odot$) which appear to be the most common in the Magellanic Clouds.

Synthetic AGB populations will be significantly modified in view of the results presented here. We have seen that the mass $M_{\rm H}(1)$ of the hydrogen-exhausted core at the first flash depends significantly on Y and Z, with $M_{\rm H}(1)$ increasing as Y increases or Z decreases. For low Z ($\lesssim 0.001$) we find $M_{\rm H}(1)$ to be a very steep function of mass for $1 \leq M/M_\odot \leq 3$, much as found for higher masses and higher metallicities. We note also that in the previous calculations of synthetic AGB populations (e.g., Iben and Truran 1978; Iben 1981; Renzini and Voli 1981) the core mass at the first pulse is, when compared to the present results, somewhat overestimated for $M \gtrsim 2\ M_\odot$ and underestimated for $M \lesssim 2\ M_\odot$. This is in the direction needed to help alleviate the low-mass part of Iben's (1981) "carbon star mystery," i.e., the lower mass models have larger initial core masses than previously believed and thus have been underestimated in their ability to become C stars. Also, the largest mass models considered in this paper show core masses which are lower than previous estimates. This reflects the effects of semiconvection and lends support to the idea that this increase in the size of the helium burning core could have led to an overestimate of the most massive stars to populate the AGB and hence an overestimate of the maximum luminosity of C stars (see Renzini *et al.* 1985; Castellani *et al.* 1985*a*, *b*).

Wood (1981) has used envelope integrations to estimate the minimum $M_{\rm H}$ for which carbon dredge-up is achieved at a given (M, Y, Z). (Although these models are yet to be confirmed by detailed stellar evolutionary calculations, they may still act as a useful guide.) He finds that the results depend significantly on the ratio α of the mixing length to the pressure scale height (see his Table 1). There is now significant evidence that theoretical calculations of the (first) giant branch of low-mass models requires $\alpha \approx 1.5$ if they are to accurately model observed giant branches (see, for example, VandenBerg 1983; Frogel, Cohen, and Persson 1983). Twarog (1978) found the same value was needed for the giant branch of NGC 188. Inclusion of molecular, and possibly grain, opacity sources will further increase the value of α necessary to obtain agreement between theory and observation.

Figure 15 shows Wood's results for $Z = 0.001$ and $Y = 0.30$, shifted to allow for an $\alpha = 1.5$. Superposed on this figure are the results of § VI*a* for $M_{\rm H}(1)$. We see immediately that any star with $M \gtrsim 1.2\ M_\odot$ should begin dredging carbon to its surface from the *first pulse*. The luminosity at this time is $M_{\rm bol} \approx -4.8$, decreasing to $M_{\rm bol} \approx -4.5$ as the mass increases to $\gtrsim 2\ M_\odot$. Wood notes that calculations with Y reduced to 0.20 indicate that carbon-enriched material is pushed further outward (i.e., to lower temperatures) at the peak of the pulse, and therefore we may expect that $M_{\rm H}^{\rm min}$, the minimum $M_{\rm H}$ for which carbon dredge-up can occur, will decrease for decreasing Y. Figure 15 indicates that for $Y = 0.20$ the $M_{\rm H}(1)$ curve intersects the $M_{\rm H}^{\rm min}$ curve (for $Y = 0.30$) at $M \approx 2\ M_\odot$. We would therefore expect stars with $M \gtrsim 2\ M_\odot$ (although this value may decrease if $M_{\rm H}^{\rm min}$ decreases for $Y = 0.20$) will begin dredging carbon to their surfaces from the first pulse, at $M_{\rm bol} \approx -4.5$. This is exactly the low-luminosity limit of Bessell, Wood, and Lloyd Evans (1983, hereafter BWLE), although the agreement should only be considered approximate because it takes a few pulses for a star to become a C star (thus increasing its luminosity), and because the low-luminosity limit can be affected by the possibility of stars being in a postflash luminosity dip. Nevertheless, the agreement is very good.

The postflash luminosity dip is by 0.5–1.0 mag for $\sim$40% of the interpulse phase (e.g., WZ; Iben 1982; Iben and Renzini 1983, 1984). It is also very likely that many, if not all, C stars are long-period variables (e.g., Miras) with light amplitudes $\Delta M_{\rm bol} \approx 0.7$ (e.g., Iben and Renzini 1983). In view of these facts it is perhaps surprising that we do not see more oxygen-rich AGB stars at higher luminosities than some C stars, as noted by Iben and Renzini. Indeed, these authors suggest that the critical luminosity for C-star formation (in the Magellanic Clouds) is $M_{\rm bol} \approx -5.0 \pm 0.2$, with any C stars having lower luminosities being in a postflash dip or near their light curve minimum. This estimate is entirely consistent with the present results, and those of Wood (1981), for $Z \approx 0.001$ and $\alpha = 1.5$. In view of these encouraging results we now look in a little more detail at three clusters believed to exhibit a metal content $Z \approx 0.001$.

Richer, Olander, and Westerlund (1979, hereafter ROW) provided details of the LMC cluster NGC 2209. There is some debate concerning the metallicity of this cluster, with the two values quoted by ROW being $Z \approx 0.001$ and $Z \approx 0.005$. We first use the equations derived from the $Z = 0.001$ calculations reported in §§ V and VI. ROW quote the turn-off mass of this cluster as being $\sim 1.6\ M_\odot$. Although a star will probably lose $\sim 0.2\ M_\odot$ during its first ascent of the giant branch, the core structure will be more like that of a 1.4 $M_\odot$ model than a 1.6 $M_\odot$ model. We therefore take the mass of the AGB stars in this cluster to be 1.6 $M_\odot$ for the determination of $M_{\rm H}(1)$. Using equation (11), and assuming $Y = 0.25$, we estimate $M_{\rm H}(1) \approx 0.62\ M_\odot$ and $M_{\rm bol} \approx -4.2$ at this time. So we expect these AGB stars to be $\sim 1.4\ M_\odot$ in mass with a hydrogen-exhausted core of $\sim 0.62\ M_\odot$. Figure 15 then tells us that this star should begin dredging carbon to its surface almost immediately. If the core mass increases by $\sim 0.05\ M_\odot$ before obtaining C-star characteristics (a conservative estimate, based on the results of Wood), then the minimum luminosity for C stars in this cluster would be, assuming full amplitude pulsation, $M_{\rm bol} \approx -5.1$. This agrees quite well with the ROW value of $M_{\rm bol} = -5.5$ for the two C stars present, which is brighter than the brightest oxygen-rich stars in the cluster (Frogel and Cohen 1982). If we use, instead, the equations from the Population I abundance models and insert $Z = 0.005$, we obtain $M_{\rm H}(1) \approx 0.58\ M_\odot$ and an initial $M_{\rm bol} \approx -3.9$ when thermal pulses begin. Interpolating in the results of Wood (1981) implies that, for $Z = 0.005$ and $\alpha = 1.5$, this model would begin to dredge

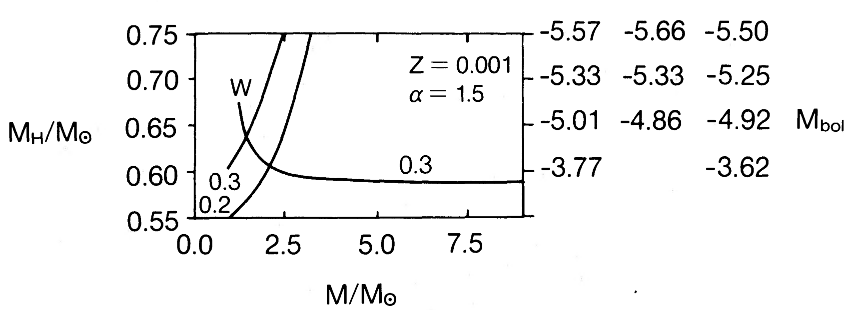

FIG. 15.—Variation, with mass, of the minimum core mass for carbon dredge-up from Wood (1981), labeled "W," and of the initial core masses at the first pulse. All curves are labeled with Y and have $Z = 0.001$. The right-hand axis gives the $M_{\rm bol}$ appropriate to the given $M_{\rm H}$. The first column gives Wood's results, for $Y = 0.30$; the second and third columns give the current results for $Y = 0.30$ and 0.20 respectively.

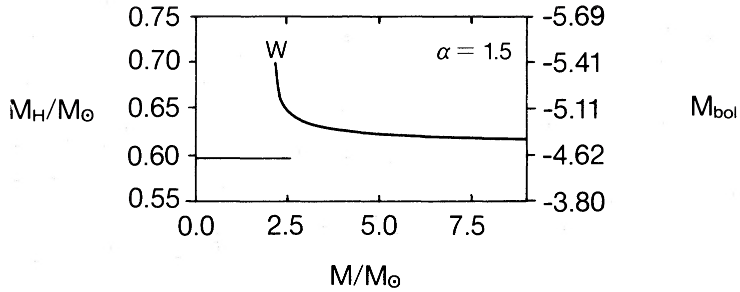

FIG. 16.—Same as Fig. 15, for $(Y, Z) = (0.30, 0.01)$. The right-hand scale is from the current results for these abundances.

carbon to its surface at $M_H \approx 0.65$ $M_\odot$ and a luminosity of $M_{bol} \approx -5.1$. Again allowing for an extra 0.05 $M_\odot$ to be added to M_H before the model becomes a C star, we would predict a minimum luminosity for C stars in this cluster of $M_{bol} \approx -5.4$. This is again in good agreement with the observed C-star luminosities of $M_{bol} \approx -5.5$ (ROW). The agreement for either value of Z is encouraging and does not rely on invoking pulsation or postflash luminosity minima (both real effects!) to match the theoretical and observed luminosities.

I now discuss two clusters considered by BWLE. First we consider the SMC cluster NGC 419. BWLE quote $Z \approx 0.002$ for this cluster and estimate the mass of stars at the turn-off to be ~ 1.3 $M_\odot$. Again we would expect the mass loss during the ascent of the first giant branch to have no real effect on the core structure, and thus although the total mass is more likely ~ 1.1 $M_\odot$ on the AGB, the initial core mass at the first pulse is probably close to $M_H(1) \approx 0.59$ $M_\odot$, calculated from equation (11) with $Y = 0.25$ and $M = 1.3$ $M_\odot$. Wood (1981) found that for $Z = 0.001$ and $Y = 0.30$ the minimum mass for dredge-up of carbon was ~ 1.13 $M_\odot$. Thus AGB stars in this cluster are just marginally capable of dredging carbon to their surface (assuming the observed luminosity is the quiescent luminosity). Thus agreement between theory and observation is again found. There are, however, two potentially troublesome C stars in this cluster with $M_{bol} \approx -4.4$, one of which is a J star. The most natural explanation for these stars is that they are currently in a postflash luminosity dip. We observe that most J stars seem to be among the brightest C stars (e.g., ROW), which is consistent with their formation via the envelope burning mechanism (e.g., Renzini and Voli 1981), provided their total mass is sufficient for this mechanism to operate. There is, however, evidence for a population of low-luminosity J stars (e.g., Richer 1981), which may be attributed to mass transfer in binary systems if $M_{bol} \gtrsim -3.5$, which is the minimum luminosity for thermal pulses to occur (Iben and Renzini 1983).

Next I look at the LMC cluster NGC 1946, estimated to have $Z \approx 0.003$ (BWLE) and a turn-off mass of ~ 1.2 $M_\odot$. The mass of stars on the AGB is thus ~ 1.0 $M_\odot$. The results of Wood (1981) indicate that even for $\alpha = 1.5$, stars of this mass will never dredge carbon to their surfaces, although a slight increase in the mass estimate would allow this to occur. The observational fact that C stars exist in this cluster (e.g., BWLE) emphasizes the importance of mass estimates for the TP-AGB stars, especially for the lower metallicities. There are two reasons for this, (1) because the initial core mass at the commencement of thermal pulsing is a steep function of the total stellar mass; and (2) because of Wood's minimum stellar mass, which is capable of the third dredge-up.

Moving to higher metallicities, Figures 16 and 17 show the minimum core mass for carbon dredge-up, M_H^{min}, from the results of Wood (1981) for $\alpha = 1.5$ and $Y = 0.30$, assuming that the shift due to increasing α from 1.0 to 1.5 is the same at $Z = 0.01$ and 0.02 as it is at $Z = 0.001$ (in many respects, e.g., giant-branch effective temperatures, the effects of increasing α increase with decreasing Z, so the M_H^{min} curves in these figures may actually be shifted a little further to the left than shown in these figures). Superposed on these figures are the approximate values for $M_H(1)$ from equations (10) and (11) for $Y = 0.30$; the values for $Y = 0.20$ are lower and fall just below the bottom of the figures. The results of Wood indicate the well-known result that, regardless of Y, α, and $M \lesssim 3$ $M_\odot$, extant theoretical models of Population I stars will not dredge carbon to their surfaces until very large core masses are attained ($M_H \gtrsim 0.7$ $M_\odot$), and even then only for masses above a lower limit (~ 2.5 $M_\odot$ for $\alpha = 1.5$; ~ 3.0 $M_\odot$ for $\alpha = 1.0$). The present results indicate that solar-like metallicity stars with $M \lesssim 2.5$ $M_\odot$ will exhibit a long history of thermal pulses before M_H reaches M_H^{min} determined by Wood, if they ever reach this limit.

Finally, I take a look at the potentially troublesome star TW Hor in NGC 1252. Bouchet (1984) gives its luminosity as 9000 $L_\odot$, $T_e = 3250$ K, and $(M, Z) = (2.2, 0.02)$. To fit this C star

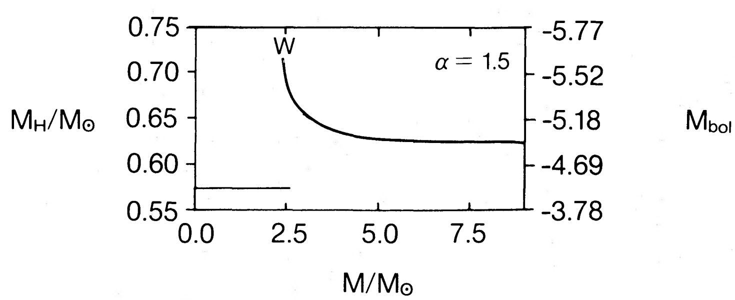

FIG. 17.—Same as Fig. 16, for $(Y, Z) = (0.30, 0.02)$

with previously published model results it was necessary to assume

1. a very low metallicity ($Z \approx 0.001$), which is inappropriate for a member of the disk;
2. that the star is currently in a postflash luminosity dip ($\sim$40% chance); or
3. that the "Iben-Renzini" mechanism operates in stars of this mass and abundance, which is far from certain, and produced C-star characteristics after ~ 1 pulse, and thus at the luminosity observed.

Taking $Y = 0.25$ and using the current models, I find $M_{\rm H}(1) \approx 0.55\ M_\odot$ at the first pulse (from eq. [10]). Equating the observed luminosity with the quiescent luminosity just prior to a pulse, equations (15) and (16) give $M_{\rm H} \approx 0.65\ M_\odot$. (If the star is in fact in a postflash luminosity dip, then this represents a lower limit to $M_{\rm H}$.) Substituting the above parameters into equation (4) for the evolutionary track gives $T_e \approx 2830$ K, which is significantly cooler than the observed 3260 K, with an estimated error of $\lesssim 200$ K (Bouchet 1984). This is consistent with the α used in the calculations being too small. Using the relation of Becker (1981), I deduce that an $\alpha \approx 1.5$ would give the observed T_e and luminosity. This is also needed to ensure that carbon is dredged to the surface, as none of the models from § VI*b*, which were evolved to full flash amplitude, showed carbon dredge-up. This is consistent with Wood's (1981) results that, in this mass range at least, an $\alpha \approx 1.5$ is needed to form C stars. Note also that the core mass for TW Hor is estimated to be $\gtrsim 0.65\ M_\odot$, which is also consistent with Wood's estimate of the minimum core mass needed for the third dredge-up to operate in stars of this mass and abundance. In conclusion, the results presented in this paper provide a natural explanation for the C star TW Hor.

The existence of low-luminosity C stars with disk metallicities, however, may pose a serious problem (e.g., Azzopardi, Lequeux, and Rebeirot 1985). If these stars are normal, single stars, then it is hard to see how they can fit current ideas about C-star formation. It would be necessary to show that the Iben-Renzini mechanism can operate efficiently at these high metallicities, or to find some other way of transporting the carbon to the stellar surface. It is also possible that some of these stars will turn out to be binaries (e.g., McClure 1985), which would mean that they would be less of an embarrasment to the theorists.

VIII. CONCLUSIONS

Although we could continue applying the current results to individual stars, the ultimate test, and one of the main reasons behind this study, is the construction of synthetic AGB populations. I have previously mentioned that the estimates of when thermal pulsing begins which were used in constructing earlier synthetic AGB distributions are changed considerably when compared to the results presented here, and that the changes are in the sense required by the observations. The dependence of $M_{\rm H}(1)$ on Z for $Z = 0.01$ and 0.001 makes interpolation between these values particularly hazardous. Yet the observations with which the models must be compared (LMC and SMC) are in this metallicity range. For this reason calculations are currently in progress for 1.0–3.0 $M_\odot$ models of these abundances. Further input from these calculations will be the dredge-up law found to operate in this mass and abundance range. Similarly, in view of the results of Wood (1981), VandenBerg (and co-workers), and the above, these calculations will use $\alpha = 1.5$.

The author wishes to thank the Monash University Computer Center, where all the calculations were performed. Special thanks to Steve Dart for coming in at weird hours and on weekends during the (brief) period when DRcaptain: was having some troubles. Thanks to Peter Wood and Bob Gingold for humoring me. Thanks also to Peter Martin, Scott Tremaine, and Dr. Ferret for helping me with TeX.

REFERENCES

Alcock, C., and Paczyński, B. 1978, *Ap. J.*, **223**, 244.
Alexander, D. R. 1975, *Ap. J. Suppl.*, **29**, 363.
Alexander, D. R., Johnson, H. R., and Rympa, R. C. 1983, *Ap. J.*, **273**, 773.
Azzopardi, M., Lequeux, J., and Rebeirot, E. 1985, *Astr. Ap.*, **145**, L6.
Barish, S. J., *et al.* 1974, *Phys. Rev. Letters*, **33**, 448.
Beaudet, G., Petrosian, V., and Salpeter, E. E. 1967, *Ap. J.*, **150**, 979.
Becker, S. A., 1981, *Ap. J. Suppl.*, **45**, 475.
———. 1982, *Ap. J.*, **260**, 695.
Becker, S. A., and Iben, I., Jr. 1979, *Ap. J.*, **232**, 831 (BI1).
———. 1980, *Ap. J.*, **237**, 111 (BI2).
Becker, S. A., Iben, I., Jr., and Tuggle, R. S. 1977, *Ap. J.*, **218**, 633 (BIT).
Bessell, M. S., Wood, P. R., and Lloyd Evans, T. 1983, *M.N.R.A.S.*, **202**, 59 (BWLE).
Blanco, B. M., Blanco, V. M., and McCarthy, M. F. 1978, *Nature*, **271**, 638.
Blanco, V. M., McCarthy, M. F., and Blanco, B. M. 1980, *Ap. J.*, **242**, 948.
Bouchet, P. 1984, *Astr. Ap.*, **139**, 344.
Cannon, R. D. 1970, *M.N.R.A.S.*, **150**, 111.
Caputo, F., Castellani, V., and Tornambè, A. 1978, *Astr. Ap.*, **67**, 107 (CCT).
Castellani, V., Chieffi, A., Pulone, L., and Tornambè, A. 1985*a*, *Ap. J.* (*Letters*), **294**, L31.
———. 1985*b*, *Ap. J.*, **296**, 204.
Castellani, V., Giannone, P., and Renzini, A. 1971*a*, *Ap. Space Sci.*, **10**, 340.
———. 1971*b*, *Ap. Space Sci.*, **10**, 355.
Castellani, V., and Tornambè, A. 1977, *Astr. Ap.*, **61**, 427 (CT).
Chiosi, C. 1986, in *Spectral Evolution of Galaxies*, ed. C. Chiosi and A. Renzini (Dordrecht: Reidel), p. 237.
Cohen, J. G., Frogel, J. A., Persson, S. E., and Elias, J. H. 1981, *Ap. J.*, **249**, 481.
Cole, P. W., and Deupree, R. G. 1980, *Ap. J.*, **239**, 284.
———. 1981, *Ap. J.*, **247**, 607.
Cox, A. N., and Stewart, J. N. 1970*a*, *Ap. J. Suppl.*, **19**, 243.
———. 1970*b*, *Ap. J. Suppl.*, **19**, 261.
Demarque, P., King, C. R., and Diaz, A. 1982, *Ap. J.*, **259**, 154.
Demarque, P., and Mengel, J. G. 1971, *Ap. J.*, **164**, 317.
———. 1972, *Ap. J.*, **171**, 583.
Despain, K. H. 1981, *Ap. J.*, **251**, 639.
Deupree, R. G. 1984*a*, *Ap. J.*, **282**, 274.
———. 1984*b*, *Ap. J.*, **287**, 268.
Deupree, R. G., and Cole, P. W. 1981, *Ap. J.* (*Letters*), **249**, L35.
———. 1983, *Ap. J.*, **269**, 676.
Dicus, D. A., Kolb, E. W., Schramm, D. N., and Tubbs, D. L. 1976, *Ap. J.*, **210**, 481.
Fahlman, G. G., Richer, H. B., and VandenBerg, D. A., 1985, *Ap. J. Suppl.*, **58**, 225.
Faulkner, D. J., and Cannon, R. D. 1973, *Ap. J.*, **180**, 435.
Festa, G., and Ruderman, M. A. 1969, *Phys. Rev.*, **180**, 1227.
Frogel, J. A., and Cohen, J. G. 1982, *Ap. J.*, **253**, 580.
Frogel, J. A., Cohen, J. G., and Persson, S. E. 1983, *Ap. J.*, **275**, 773.
Frogel, J. A., Persson, S. E., and Cohen, J. G. 1980, *Ap. J.*, **239**, 495.
Fujimoto, M. Y., Nomoto, K., and Sugimoto, D. 1976, *Pub. Astr. Soc. Japan*, **28**, 89.
Fujimoto, M. Y., and Sugimoto, D. 1979, *Pub. Astr. Soc. Japan*, **31**, 1.
Gabriel, M. 1970, *Astr. Ap.*, **6**, 124.
Gingold, R. A. 1974, *Ap. J.*, **193**, 177.
———. 1975, *Ap. J.*, **198**, 425.
———. 1976, *Ap. J.*, **204**, 116.
Härm, R., and Schwarzschild, M. 1966, *Ap. J.*, **145**, 496.
Hasert, F. J., *et al.* 1973, *Phys. Letters*, **46B**, 121.
Havazelet, D., and Barkat, Z. 1979, *Ap. J.*, **233**, 589.
Hollowell, D. 1986, in *Proc. Calgary Workshop on Late Stages of Stellar Evolution*, in press.
Huebner, W. F., Merts, A. L., Magee, N. H., Jr., and Argo, M. F. 1977, *Los Alamos Scientific Laboratory Rept.*, No. LA-6760-M.
Iben, I., Jr. 1975*a*, *Ap. J.*, **196**, 525.
———. 1975*b*, *Ap. J.*, **196**, 549.
———. 1976, *Ap. J.*, **208**, 165.
———. 1977, *Ap. J.*, **217**, 788.
———. 1981, *Ap. J.*, **246**, 278.
———. 1982, *Ap. J.*, **260**, 821.
———. 1984, in *IAU Symposium 105, Observational Tests of the Stellar Evolution Theory*, ed. A. Maeder and A. Renzini (Dordrecht: Reidel), p. 3.

Iben, I., Jr., and Renzini, A. 1982*a*, *Ap. J.* (*Letters*), **259**, L79.
———. 1982*b*, *Ap. J.* (*Letters*), **263**, L188.
———. 1983, *Ann. Rev. Astr. Ap.*, **21**, 271.
———. 1984, *Phys. Rept.*, **105**, 329.
Iben, I., Jr., and Rood, R. T. 1970, *Ap. J.*, **161**, 587.
Iben, I., Jr., and Truran, J. W. 1978, *Ap. J.*, **200**, 980.
Itzykson, C., and Zuber, J.-B. 1980, *Quantum Field Theory* (New York: McGraw-Hill).
Kippenhahn, R. 1981, *Astr. Ap.*, **102**, 293.
Lattanzio, J. C. 1984*a*, Ph.D. thesis, Monash University.
———. 1984*b*, *M.N.R.A.S.*, **207**, 309.
Lauterborn, D., Refsdal, S., and Weigert, A. 1971, *Astr. Ap.*, **10**, 97.
Lubkin, G. B. 1978, *Phys. Today*, Vol. **31**, No. 9, p. 17.
McClure, R. D. 1985, *J. Roy. Astr. Soc. Canada*, **79**, 277.
Miller, G. E., and Scalo, J. 1982, *Ap. J.*, **263**, 259.
Mould, J., and Aaronson, M. 1979, *Ap. J.*, **232**, 421.
———. 1980, *Ap. J.*, **240**, 464.
Paczyński, B. 1970, *Acta Astr.*, **20**, 47.
———. 1971, *Acta Astr.*, **21**, 417.
———. 1974, *Ap. J.*, **192**, 483.
———. 1975, *Ap. J.*, **202**, 558.
Ramadurai, S. 1976, *M.N.R.A.S.*, **176**, 9.
Renzini, A., Bernazanni, M., Buonanno, R., and Corsi, C. E. 1985, *Ap. J.* (*Letters*), **294**, L7.
Renzini, A., and Voli, M. 1981, *Astr. Ap.*, **94**, 175.
Richer, H. B. 1981, *Ap. J.*, **243**, 744.
Richer, H. B., Olander, N., and Westerlund, B. E. 1979, *Ap. J.*, **230**, 724 (ROW).
Robertson, J. W. 1971, *Ap. J.*, **170**, 353.
Robertson, J. W., and Faulkner, D. J. 1972, *Ap. J.*, **171**, 309.
Sackmann, L.-J. 1977, *Ap. J.*, **212**, 159.
———. 1980, *Ap. J.*, **235**, 960.
Salam, A. 1968, in *Elementary Particle Theory*, ed. N. Svartholm (Stockholm: Almquist and Wilksells), p. 366.
Scalo, J., and Miller, G. E. 1981, *Ap. J.*, **246**, 251.
Schwarzschild, M., and Härm, R. 1967, *Ap. J.*, **150**, 961.
Sugimoto, D., and Fujimoto, M. Y. 1978, *Pub. Astr. Soc. Japan*, **30**, 467.
Sweigart, A. V., and Demarque, P. 1972, *Astr. Ap.*, **20**, 445.
———. 1973, in *Variable Stars in Globular Clusters and Related Systems*, ed. J. D. Fernie (Dordrecht: Reidel), p. 221.
Sweigart, A. V., and Gross, P. G. 1976, *Ap. J. Suppl.*, **32**, 367.
———. 1978, *Ap. J. Suppl.*, **36**, 405.
Sweigart, A. V., and Renzini, A. 1979, *Astr. Ap.*, **71**, 66.
Taam, R. E., Kraft, R. D., and Suntzeff, N. 1976, *Ap. J.*, **207**, 201.
Tuchman, Y., Glasner, A., and Barkat, Z. 1983, *Ap. J.*, **268**, 356.
Twarog, B. A. 1978, *Ap. J.*, **220**, 890.
VandenBerg, D. A. 1983, *Ap. J. Suppl.*, **51**, 29.
———. 1985, *Ap. J. Suppl.*, **58**, 711.
VandenBerg, D. A., and Bell, R. A. 1985, *Ap. J. Suppl.*, **58**, 561.
VandenBerg, D. A., and Bridges, T. J. 1984, *Ap. J.*, **278**, 679.
VandenBerg, D. A., Hartwick, F. D. A., Dawson, P., and Alexander, D. A. 1983, *Ap. J.*, **266**, 747.
VandenBerg, D. A., and Hrivnak, B. J. 1985, *Ap. J.*, **291**, 270.
Weinberg, S. 1967, *Phys. Rev. Letters*, **19**, 1264.
———. 1972, *Phys. Rev. Letters*, **27**, 1688.
Wood, P. R. 1981, in *Physical Processes in Red Giants*, ed. I. Iben, Jr., and A. Renizini (Dordrecht: Reidel), p. 135.
Wood, P. R., and Cahn, J. H. 1977, *Ap. J.*, **211**, 499.
Wood, P. R., and Zarro, D. M. 1981, *Ap. J.*, **247**, 247 (WZ).

Note added in proof 1986 September 5.—Models have been calculated for $Z = 0.003$ and 0.006 with $\alpha = 1.5$ and show dredge-up of carbon can occur for $M_{\mathrm{H}} \gtrsim 0.62\ M_{\odot}$. One of the models became a carbon star with a core mass of only 0.65 $M_{\odot}$ and $M_{\mathrm{bol}} = -4.4$. The pulse which produced C > O had $\lambda = \Delta M_{\mathrm{dredge}}/\Delta M_{\mathrm{H}} = 0.38$.

JOHN C. LATTANZIO: Canadian Institute for Theoretical Astrophysics, McLennan Physical Laboratories, University of Toronto, 60 St. George Street, Toronto, Ontario M5S 1A1, Canada